

NACA RM L58B28

**NACA**

# RESEARCH MEMORANDUM

AN EXPLORATORY INVESTIGATION AT MACH NUMBERS OF 2.50  
AND 2.87 OF A CANARD BOMBER-TYPE CONFIGURATION  
DESIGNED FOR SUPERSONIC CRUISE FLIGHT

By Thomas C. Kelly, Melvin M. Carmel, and Donald T. Gregory

Langley Aeronautical Laboratory  
Langley Field, Va.

CLASSIFICATION CHANGED

**LIBRARY COPY**

UNCLASSIFIED

APR 15 1958

LANGLEY AERONAUTICAL LABORATORY  
LIBRARY, NACA  
LANGLEY FIELD, VIRGINIA

Authority of *NASA Htr* Dated *Aug. 9, 1963*,  
CLASSIFIED DOCUMENT

This material contains information affecting the National Defense of the United States within the meaning of the espionage laws, Title 18, U.S.C., Secs. 793 and 794, the transmission or revelation of which in any manner to an unauthorized person is prohibited by law.

*HQ. Maines*  
*HR-9-25-63*  
**NATIONAL ADVISORY COMMITTEE  
FOR AERONAUTICS**

WASHINGTON

April 15, 1958

~~CONFIDENTIAL~~

AUG 11 1958

THIS PAGE IS UNCLASSIFIED

ERRATA

NACA Research Memorandum L58B28

By Thomas C. Kelly, Melvin M. Carmel, and Donald T. Gregory  
April 1958

Page 5:

In lines 10 and 11, change 31 to 30.  
In line 12, change 62 to 60.

Page 13: The following items in table I should be corrected:

Wing:

Mean aerodynamic chord, in. - change 27 to 27.04.

Ventral fins:

Area, each, sq in. - change 25.78 to 26.08.

Vertical fins:

Area, each, sq in. - change 30.92 to 30.08.  
Root chord, in. - change 9.43 to 9.03.  
Aspect ratio - change 0.851 to 0.875.  
Taper ratio - change 0.289 to 0.299.  
Mean aerodynamic chord - change 6.69 to 6.44.

Center-of-gravity location -

Percent of mean aerodynamic chord - change 24 to 21.4.

Page 15, Figure 2(a):

In the plan-form view, the dimension labeled 40.75 from nose to  $\bar{c}/4$  should be 41.35.

The spanwise dimension to  $\bar{c}$  labeled 4.785 should be 5.06.

The label  $\bar{c} = 27.0$  should be  $\bar{c} = 27.04$ .

The dimension 6.75 between the leading edge and  $\bar{c}/4$  should be 6.76.

Page 16, Figure 2(b):

The dimension for the root chord, shown as 9.43, should be 9.03. This dimension should not go to the wing-section trailing edge, as shown, but to the vertical-tail trailing edge extended to the wing-section lower surface.

THIS PAGE IS UNCLASSIFIED

## NATIONAL ADVISORY COMMITTEE FOR AERONAUTICS

## RESEARCH MEMORANDUM

AN EXPLORATORY INVESTIGATION AT MACH NUMBERS OF 2.50

AND 2.87 OF A CANARD BOMBER-TYPE CONFIGURATION

DESIGNED FOR SUPERSONIC CRUISE FLIGHT

By Thomas C. Kelly, Melvin M. Carmel, and Donald T. Gregory

## SUMMARY

Results have been obtained in the Langley Unitary Plan wind tunnel at Mach numbers of 2.50 and 2.87 and Reynolds numbers of  $3.06 \times 10^6$  and  $2.52 \times 10^6$ , respectively, for a canard bomber-type configuration designed for supersonic cruise flight. Tests extended over an angle-of-attack range from about  $-4^\circ$  to  $11^\circ$  and an angle-of-sideslip range from  $-4^\circ$  to  $6^\circ$ .

These results indicated that the original configuration had a trimmed maximum lift-drag ratio that varied from about 6.1 at a Mach number of 2.50 to 5.8 at a Mach number of 2.87. The untrimmed maximum lift-drag ratios were 6.4 and 6.2 at Mach numbers of 2.50 and 2.87. The reductions in maximum lift-drag ratio due to trimming result from increases in drag associated with the significant canard incidence angles required for trim at lift coefficients near those for maximum lift-drag ratio. Significant canard incidence angles are required, for the most part, to overcome a large negative pitching moment which exists for this configuration at zero lift.

Although the original configuration was directionally unstable at low angles of attack, satisfactory directional stability could be obtained by the addition of single or double upper-surface vertical fins with only slight penalties in maximum lift-drag ratio.

## INTRODUCTION

The need for a bomber-type aircraft having an increased retaliatory capability has led to the concept of a long-range all-supersonic cruise configuration. Such an aircraft would represent a considerable improvement over present-day bomber aircraft which obtain range by cruising at high subsonic speeds, utilizing a supersonic dash to the target.

Recent design studies have indicated that the use of the newer, high-energy fuels in combination with advanced engine designs and improved aerodynamic design adds to the probability of developing a practical configuration having suitable range and an all-supersonic mission profile.

The Langley Laboratory of the NACA has accordingly initiated an accelerated research program designed to provide information on various factors affecting flight at Mach numbers near 3.0. As one phase of this program, several configurations, proposed for cruise flight at Mach numbers near 3.0, have been designed and tested.

The present paper contains results obtained for a canard bomber configuration designed to obtain high lift-drag ratios through the use of favorable lift interference. Initial, exploratory, tests have been conducted at the Langley Unitary Plan wind tunnel at Mach numbers of 2.50 and 2.87 and at corresponding Reynolds numbers of  $3.06 \times 10^6$  and  $2.52 \times 10^6$  based on the wing mean aerodynamic chord. Tests extended over an angle-of-attack range from approximately  $-4^\circ$  to  $11^\circ$  and an angle-of-sideslip range from approximately  $-4^\circ$  to  $6^\circ$ . Results are presented with only brief analysis in order to expedite publication.

The original configuration consisted of a clipped-delta plan-form wing in combination with a full-delta canard surface. An engine package, mounted beneath the flat lower surface of the wing, was designed to produce a high-pressure field over the wing lower surface. Ventral fins were attached to the wing tips to provide lateral stability and control and to augment the interference lift generated by the engine package.

Several previous investigations have indicated some of the advantages and disadvantages associated with the canard configuration. (See refs. 1 to 4, for example.)

#### SYMBOLS

The aerodynamic force and moment data are referred to the stability axes (fig. 1) with the origin at the center of gravity. The symbols used are defined as follows:

$b$  wing span, in.

$\bar{c}$  mean aerodynamic chord of wing, in.

$C_D^i$  drag coefficient,  $\frac{F_D}{q_\infty S}$

$C_{D_b}^i$  base drag coefficient,  $\frac{\text{Base drag}}{q_\infty S}$

$C'_{Dc}$	chamber drag coefficient, $\frac{\text{Chamber drag}}{q_{\infty} S}$
$C'_{Di}$	internal-duct drag coefficient, $\frac{\text{Internal-duct drag}}{q_{\infty} S}$
$C'_{Dr}$	ramp-pressure (boundary-layer-diverter) drag coefficient
$C_L$	lift coefficient, $\frac{F_L}{q_{\infty} S}$
$C_{L,s}$	rolling-moment coefficient, $\frac{\text{Rolling moment}}{q_{\infty} S b}$
$C_m$	pitching-moment coefficient, $\frac{\text{Pitching moment}}{q_{\infty} S \bar{c}}$
$C_{n,w}$	yawing-moment coefficient, $\frac{\text{Yawing moment}}{q_{\infty} S b}$
$C_Y$	side-force coefficient, $\frac{F_Y}{q_{\infty} S}$
$F_D$	drag force, lb
$F_L$	lift force, lb
$F_Y$	side force, lb
$(L/D)_{\max}$	maximum lift-drag ratio
$M$	free-stream Mach number
$q_{\infty}$	free-stream dynamic pressure, lb/sq ft
$S$	wing area, sq ft

- $\alpha$  angle of attack of bottom surface of wing, deg
- $\beta$  angle of sideslip of fuselage center line, deg
- $\delta_c$  canard angle, measured with respect to wing lower surface,  
positive when leading edge is up, deg

$$C_{L\alpha} = \frac{\partial C_L}{\partial \alpha}, \text{ per deg}$$

$$C_{L\beta} = \frac{\partial C_L}{\partial \beta}, \text{ per deg}$$

$$C_{mC_L} = \frac{\partial C_m}{\partial C_L}$$

$$C_{m\delta_c} = \frac{\partial C_m}{\partial \delta_c}, \text{ per deg}$$

$$C_{n\beta} = \frac{\partial C_n}{\partial \beta}, \text{ per deg}$$

$$C_{Y\beta} = \frac{\partial C_Y}{\partial \beta}, \text{ per deg}$$

## APPARATUS AND TESTS

### Tunnel

Tests were conducted in the low Mach number test section of the Langley Unitary Plan wind tunnel, which is a variable pressure, continuous-flow tunnel. The nozzle leading to the test section is of the asymmetric, sliding-block type, which permits a continuous variation in test section Mach number from about 1.5 to 2.9.

### Model

A three-view drawing and the design dimensions of the model tested are shown in figure 2(a) and in table I, respectively.

The wing has a clipped-delta plan form, the rear outboard portions consisting of elevons for longitudinal and lateral control. For these tests the elevons were fixed at  $0^\circ$ . Wedge-sectioned ventral fins are attached to the wing tips for purposes of lateral stability and control and also to take advantage of favorable lift interference. The outboard surfaces of the ventral fins are parallel to the airstream. Additional vertical fin surfaces, tested with the original configuration, were installed in combination with the ventral fins. A single vertical fin was installed on the body center line and double vertical fins at  $0.3b/2$ . Each vertical fin had an area of about 31 square inches; therefore, with the added fin on the body center line, about 31 square inches of area were added, and with the fins at  $0.3b/2$ , about 62 square inches were added.

The canard control surface has a delta plan form with provision made to test the canard at angles of deflection (relative to the wing lower surface) of  $0^\circ$ ,  $5^\circ$ , and  $10^\circ$ ; the hinge line of the canard was at 67 percent of the canard-body juncture chord.

The body of the configuration varies in cross section from a 2 to 1 ellipse over the forward portion to a combination of a half-ellipse and rectangle farther rearward. The upper body line fairs into the wing upper surface at the maximum thickness station. (See fig. 2(a).)

The overall height and width of the engine package were determined by consideration of full-scale engine dimensions. This package, which is attached to the wing lower surface (fig. 2(a)), consists of ducting to provide simulated air flow through an engine system and a boundary-layer diverter. Because the model test Reynolds numbers were considerably lower than those which would be experienced in full-scale flight, the proportion of diverter depth to overall package depth for the model is greater than that which would be required on a full-scale airplane. Since the engine-package overall dimensions were fixed, the relatively large boundary-layer diverter resulted in a reduction in model inlet area from a value compatible with the proposed full-scale six-engine system. The model duct exits, in turn, were sized to the duct inlet area in order to achieve sonic flow at the duct exit and thereby facilitate computations of internal drag. The model base, therefore, is not intended to suggest an engine-package base that would be used on a full-scale configuration. Photographs of the model are shown in figure 3.

#### Test Conditions and Procedure

The tests were performed at a stagnation pressure of approximately 8 pounds per square inch absolute and a stagnation temperature of  $150^\circ\text{F}$ . The dewpoint, measured at stagnation pressure, was maintained below  $-30^\circ\text{F}$  in order to assure negligible condensation effects.

All configurations were tested at Mach numbers of 2.50 and 2.87; corresponding Reynolds numbers were  $3.06 \times 10^6$  and  $2.52 \times 10^6$ . The angle-of-attack range varied from approximately  $-4^\circ$  to  $11^\circ$ , and the angle-of-sideslip range varied from about  $-4^\circ$  to  $6^\circ$ . Characteristics of the model in sideslip were obtained at angles of attack of approximately  $1.1^\circ$ ,  $5.5^\circ$ , and  $12^\circ$  at a Mach number of 2.50 and at  $0.2^\circ$ ,  $4.4^\circ$ , and  $10.7^\circ$  at a Mach number of 2.87.

The tests were conducted with natural boundary-layer transition. However, unpublished results from more recent tests indicate the presence of turbulent flow even for the condition of natural transition.

### Measurements

Aerodynamic forces and moments were determined by means of a six-component electrical strain-gage balance housed within the engine package. The balance, in turn, was rigidly fastened to a sting support system and provision was made to detect any fouling between the model and sting support system.

Balance chamber pressure was measured with a single static orifice located in the vicinity of the strain-gage balance. Base pressure measurements were made on one side of the model base only, using two multi-orifice tubes which encircled approximately equal segments of the model base. Pressures from these tubes were averaged. Duct exit pressures were determined on one side of the model base by means of four-tube total-pressure rakes placed in each of the three circular exits. Each rake was manifolded to a single tube in order to provide an average total pressure for the duct exit. A check to determine the existence of sonic flow at the duct exit was made by means of a static pressure measurement at one of the duct exits.

Pressure-distribution measurements were also obtained along the wall and floor of the boundary-layer ramp in an attempt to estimate the drag penalty imposed by this type of diverter. All pressures except those for the boundary-layer diverter were measured at each test point.

Schlieren photographs of each of the model configurations were taken at various attitudes and Mach numbers.

### Corrections

Although calibration of the tunnel test section has not been completed, measured pressure gradients have indicated that model buoyancy effects would be negligible. Corrections to the indicated model angle

of attack have been made for both tunnel air-flow misalignment and deflection of model and sting support due to load.

The drag data presented herein have been adjusted to correspond to zero balance chamber and base drag coefficients. In addition, the internal, or duct drag, has been subtracted from the adjusted drag values and the drag coefficients presented in this paper represent the net external drag of the model.

#### Accuracy

Based upon balance calibration and repeatability of data, it is estimated that the various measured quantities are accurate within the following limits at low lift coefficients:

$C_L$	±0.004
$C_D'$	±0.001
$C_{D_b}'$	±0.0002
$C_{D_c}'$	±0.0002
$C_{D_i}'$	±0.0002
$C_m$	±0.001
$C_{l,s}$	±0.0002
$C_{n,w}$	±0.0005
$C_Y$	±0.002
$\alpha$ , deg	±0.15
$\beta$ , deg	±0.10

The maximum deviation of local Mach number from the free-stream values given is ±0.015.

## PRESENTATION OF RESULTS

Results of this investigation are presented in the following figures:

	Figure
Typical schlieren photographs of original model . . . . .	4
Variation of internal, chamber, base, and boundary-layer-diverter drag coefficients with angle of attack . . . . .	5
Effect of canard on aerodynamic characteristics in pitch . . . . .	6
Effect of ventral and vertical fins on aerodynamic characteristics in pitch . . . . .	7
Effect of ventral and vertical fins on aerodynamic characteristics in sideslip, $M = 2.50$ . . . . .	8
Effect of ventral and vertical fins on aerodynamic characteristics in sideslip, $M = 2.87$ . . . . .	9
Summary of aerodynamic characteristics in pitch . . . . .	10
Variation of trimmed $L/D$ with lift coefficient . . . . .	11
Variation of canard effectiveness parameter with Mach number for several lift coefficients . . . . .	12
Variation with angle of attack of the static lateral and directional stability derivatives . . . . .	13

It should be noted that the curves presented in figures 10 and 12 were obtained from points taken at Mach numbers 2.50 and 2.87 only. The actual variations with Mach number, therefore, may differ somewhat from those shown in the figures.

## DISCUSSION

## Longitudinal Characteristics

Drag.- Minimum drag coefficients for the original model (fig. 6) at Mach numbers of 2.50 and 2.87 are about 0.0130 for the model with the canard at an incidence angle of  $0^\circ$ . Maximum lift-drag ratios for this

configuration vary from about 6.4 to 6.2 as Mach number is increased from 2.50 to 2.87 (fig. 10). Removing the canard, or increasing the canard angle to  $5^\circ$  results in only slight variations in drag at low lift coefficients (fig. 6). Further increases in canard angle to  $10^\circ$  result in substantial increases in drag.

The maximum values of trimmed lift-drag ratio (fig. 11) are about 6.1 and 5.8 for Mach numbers of 2.50 and 2.87, respectively. Corresponding lift coefficients for these values of trimmed  $(L/D)_{\max}$  are about 0.145 and 0.132, respectively.

The addition of vertical fins at either the body center line or at  $0.3b/2$  has only a slight effect on minimum drag, and causes a 5-percent reduction in  $(L/D)_{\max}$  at a Mach number of 2.87. (See figs. 7 and 10.) Removal of the ventral fins slightly reduces the minimum drag coefficient (fig. 7), but has little or no effect on maximum lift-drag ratio (fig. 10).

Consideration of the magnitude of the drag coefficient for the original configuration indicates that the drag resulting from the energy loss of the air flowing through the boundary-layer diverter amounts to approximately 8 percent of the total. The full-scale-airplane diverter drag would probably not be this large, inasmuch as its boundary layer is relatively thinner and a smaller diverter would be required.

Lift.— Results presented in figure 6 indicate that the original model exhibits positive lift at an angle of attack of  $0^\circ$ . It is believed that much of the lift increment shown comes from a positive pressure field generated on the wing lower surface by the engine package. It is interesting to note (fig. 7) that the ventral fins apparently contain this positive pressure field somewhat, thereby augmenting the interference lift caused by the presence of the engine package. This effect is most noticeable at a Mach number of 2.50.

Figure 10 indicates that canard angle has only a slight effect on lift-curve slope. As would be expected, removal of the canard results in a noticeable decrease in lift-curve slope. Also, the lift increases slightly with an increase in canard incidence angle; therefore, trim lift-curve slopes for these configurations would be higher than those shown in figure 10 which are for untrimmed conditions.

Pitching moment.— The center-of-gravity location used for the present tests, which was at the approximate model center of volume, was selected to give a value of  $\partial C_m / \partial C_L$  of about -0.05 at a Mach number of 2.87 (fig. 10). It should be noted here that unpublished data indicate that this center-of-gravity location would lead to longitudinal instability at subsonic Mach numbers. Therefore, it may be necessary

to consider either moving the center-of-gravity location or folding the canard in order to provide a stable configuration for subsonic flight.

The pitching-moment curves shown in figure 6 are interesting in that they consist basically of two linear portions, with a stabilizing break occurring at lift coefficients near those for  $(L/D)_{\max}$ . This suggests the possibility of having a configuration which may be made very nearly neutrally stable for cruise conditions with sufficient stability available for maneuvering flight.

Figure 6 also shows that with the canard at an angle of incidence of  $0^\circ$ , a negative pitching moment occurs at zero lift, resulting in the requirement that large canard angles be used for trim at lift coefficients near those for  $(L/D)_{\max}$ . The large canard incidence angles lead, in turn, to substantial reductions in maximum lift-drag ratios. (See figs. 10 and 11.) This adverse condition would be further aggravated at higher Mach numbers because of the decrease in canard power (fig. 12). As previously mentioned, small changes in canard incidence have little or no effect on maximum lift-drag ratio, thus indicating that the canard can be an efficient longitudinal control for a properly designed configuration. One method of obtaining zero or positive pitching moment at zero lift would be redesign of the wing section. Results presented in reference 5 also indicate that modification to the forebody may be made in such a way that positive pitching-moment shifts may be obtained with little or no change in drag.

#### Lateral Stability

Results presented in figures 8, 9, and 13 indicate that the original model with the ventral fins removed is directionally unstable at all angles of attack at both Mach numbers. Addition of the ventral fins has a significant stabilizing effect; however, the original model is still directionally unstable at angles of attack less than about  $4\frac{1}{2}^\circ$  at a Mach number of 2.50 and  $6^\circ$  at a Mach number of 2.87. The directional stability decreases with an increase in Mach number and, for the original configuration with its vertical-surface area all in ventral form, increases with an increase in angle of attack. (See fig. 13.) Further addition of either the single or double upper-surface vertical fins provides configurations that are directionally stable throughout the angle-of-attack range tested at both Mach numbers.

It is interesting to note in figure 13 that at angles of attack near  $0^\circ$  the double upper-surface vertical fins contribute an increment

in directional stability which is approximately twice that indicated for the single vertical fin. At a Mach number of 2.87, the increment due to the addition of the double upper-surface fins remains almost constant throughout the angle-of-attack range, whereas the increment associated with the single fin decreases with angle of attack and approaches zero at angles of attack near  $10^\circ$ . It is believed that the variations shown are related to the sidewash field originating at the wing-body juncture. (See ref. 6.)

Figure 13 also shows that all test configurations exhibit positive effective dihedral. As would be expected, the ventral fins reduce the dihedral effect somewhat.

#### CONCLUDING REMARKS

Results of an investigation of a canard bomber-type configuration at Mach numbers of 2.50 and 2.87 indicate the following:

The original configuration had a trimmed maximum lift-drag ratio which varied from about 6.1 at a Mach number of 2.50 to 5.8 at a Mach number of 2.87 at corresponding test Reynolds numbers of  $3.06 \times 10^6$  and  $2.52 \times 10^6$ . Untrimmed maximum lift-drag ratios were 6.4 and 6.2 at Mach numbers of 2.50 and 2.87, respectively. The reductions in maximum lift-drag ratio due to trimming result from increases in drag associated with the significant canard incidence angles required for trim at lift coefficients near those for maximum lift-drag ratios. Significant canard incidence angles are required, for the most part, to overcome a large negative pitching moment which exists for this configuration at zero lift. It is felt that modification of the model forebody may be made in such a manner as to obtain positive shifts in pitching moment with little or no change in drag so that smaller canard angles would be required for trim.

Although the original configuration was directionally unstable at low angles of attack, satisfactory directional stability could be obtained by the addition of upper-surface vertical fins with only small penalties in maximum lift-drag ratio.

Langley Aeronautical Laboratory,  
National Advisory Committee for Aeronautics,  
Langley Field, Va., February 13, 1958.

## REFERENCES

1. Driver, Cornelius: Longitudinal and Lateral Stability and Control Characteristics of Two Canard Airplane Configurations at Mach Numbers of 1.41 and 2.01. NACA RM L56L19, 1957.
2. Mathews, Charles W.: Study of the Canard Configuration With Particular Reference to Transonic Flight Characteristics and Low-Speed Characteristics at High Lift. NACA RM L8G14, 1949.
3. Johnson, Joseph L., Jr., and Paulson, John W.: Free-Flight-Tunnel Investigation of the Low-Speed Stability and Control Characteristics of a Canard Airplane Model. NACA RM L53I11, 1953.
4. Bates, William R.: Low-Speed Static Longitudinal Stability Characteristics of a Canard Model Having a  $60^\circ$  Triangular Wing and Horizontal Tail. NACA RM L9H17, 1949.
5. Spearman, M. Leroy: Some Factors Affecting the Static Longitudinal and Directional Stability Characteristics of Supersonic Aircraft Configurations. NACA RM L57E24a, 1957.
6. Spearman, M. Leroy, and Driver, Cornelius: Longitudinal and Lateral Stability and Control Characteristics at Mach Number 2.01 of a  $60^\circ$  Delta-Wing Airplane Configuration Equipped With a Canard Control and With Wing Trailing-Edge Flap Controls. NACA RM L58A20, 1958.

TABLE I.- MODEL DESIGN DIMENSIONS

## Wing:

Area, sq ft . . . . .	4.183
Span, in. . . . .	23.33
Root chord, in. . . . .	36.00
Tip chord, in. . . . .	15.73
Aspect ratio . . . . .	0.904
Taper ratio . . . . .	0.437
Mean aerodynamic chord, in. . . . .	27.00
Leading-edge sweep, deg . . . . .	62
Airfoil section . . . . .	Double wedge, flat lower surface
Thickness-chord ratio (with maximum thickness at 70 percent chord) . . . . .	0.025

## Canard:

Area (total), sq ft . . . . .	0.700
Area (exposed), sq ft . . . . .	0.370
Span, in. . . . .	14.66
Root chord, in. . . . .	13.75
Tip chord . . . . .	0
Aspect ratio . . . . .	2.13
Taper ratio . . . . .	0
Mean aerodynamic chord, in. . . . .	9.17
Leading-edge sweep, deg . . . . .	62
Airfoil section . . . . .	Double wedge
Thickness-chord ratio (with maximum thickness at 70 percent chord) . . . . .	0.025

## Ventral fins:

Area, each, sq in. . . . .	25.78
Airfoil section . . . . .	Single wedge

## Vertical fins:

Area, each, sq in. . . . .	30.92
Height, in. . . . .	5.13
Root chord, in. . . . .	9.43
Tip chord, in. . . . .	2.70
Aspect ratio . . . . .	0.851
Taper ratio . . . . .	0.289
Mean aerodynamic chord, in. . . . .	6.69
Leading-edge sweep, deg . . . . .	62
Airfoil section . . . . .	Double wedge
Thickness-chord ratio (with maximum thickness at 70 percent chord) . . . . .	0.025

## Center-of-gravity location -

Percent overall length . . . . .	64
Percent of mean aerodynamic chord . . . . .	24

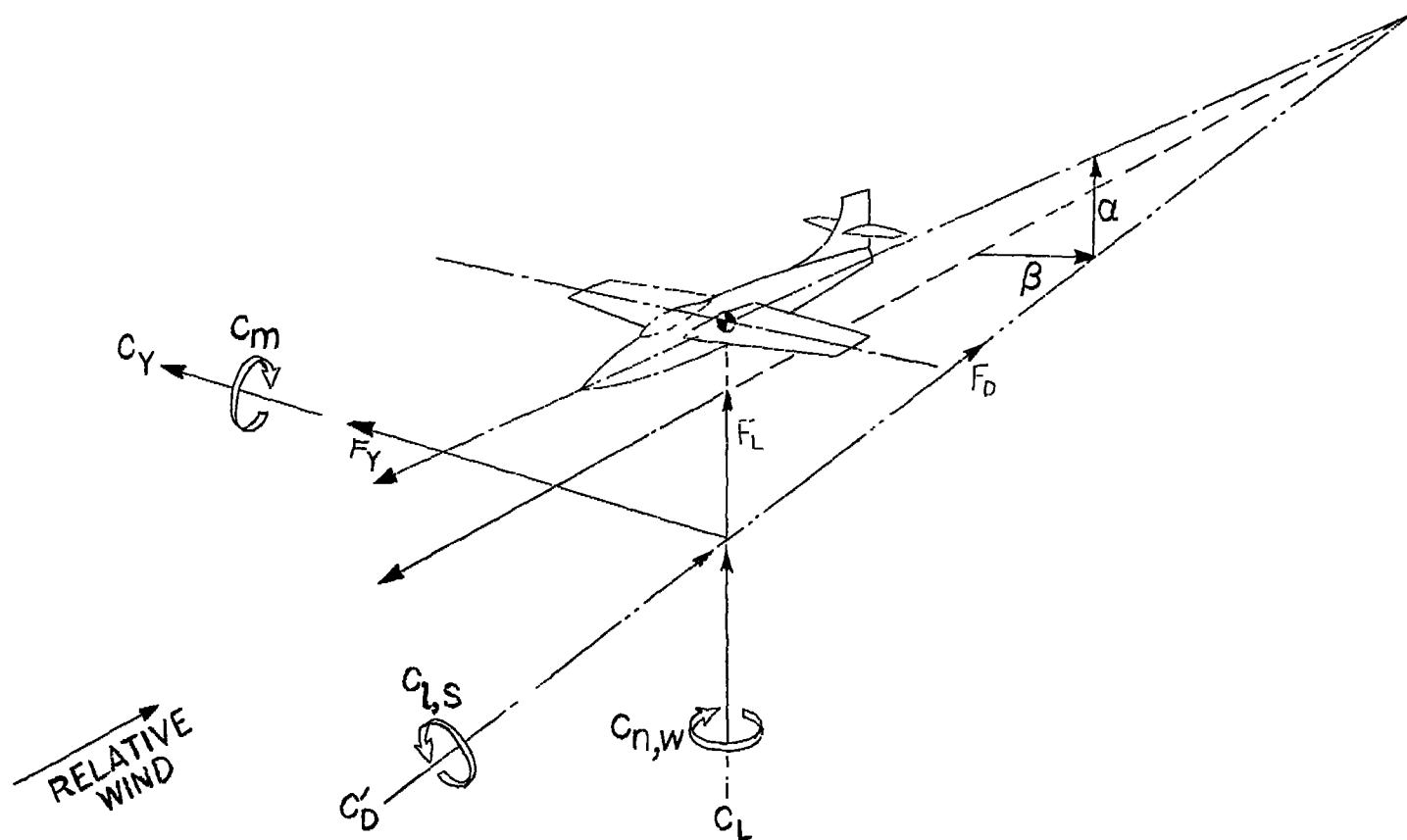
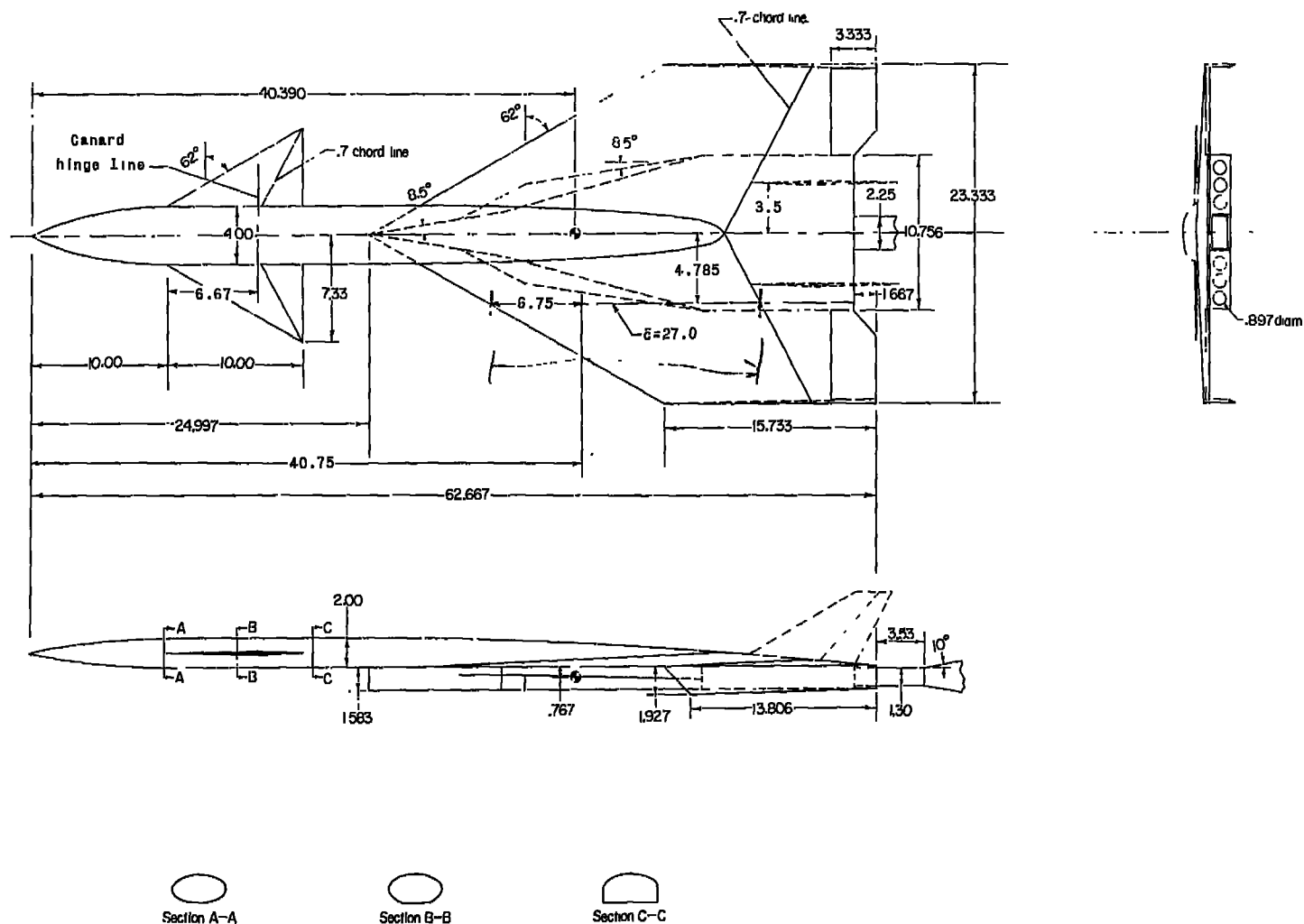
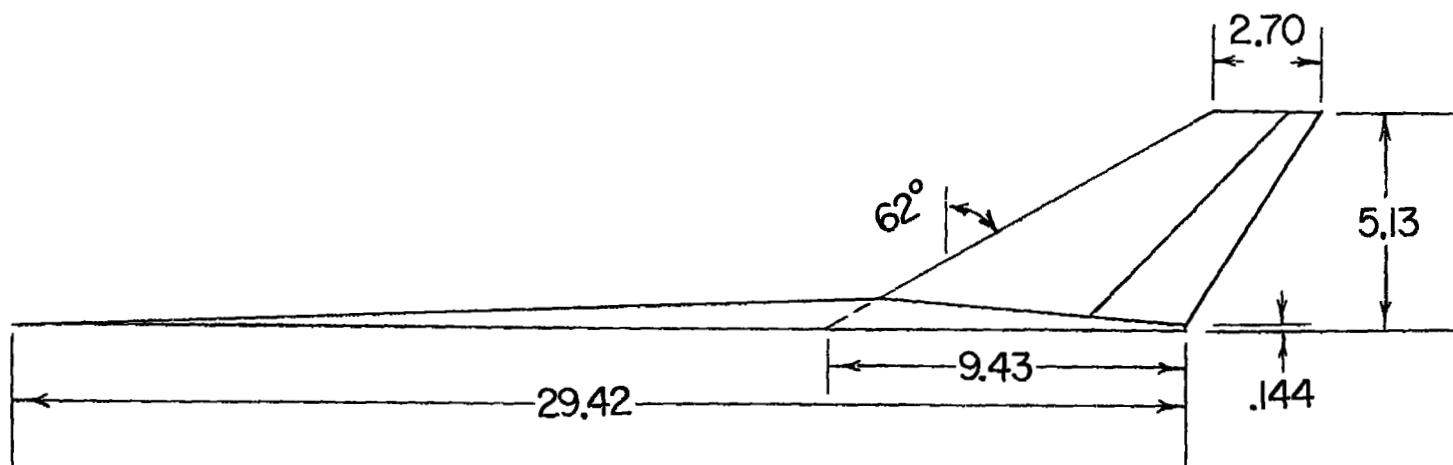


Figure 1.- Stability axes system.



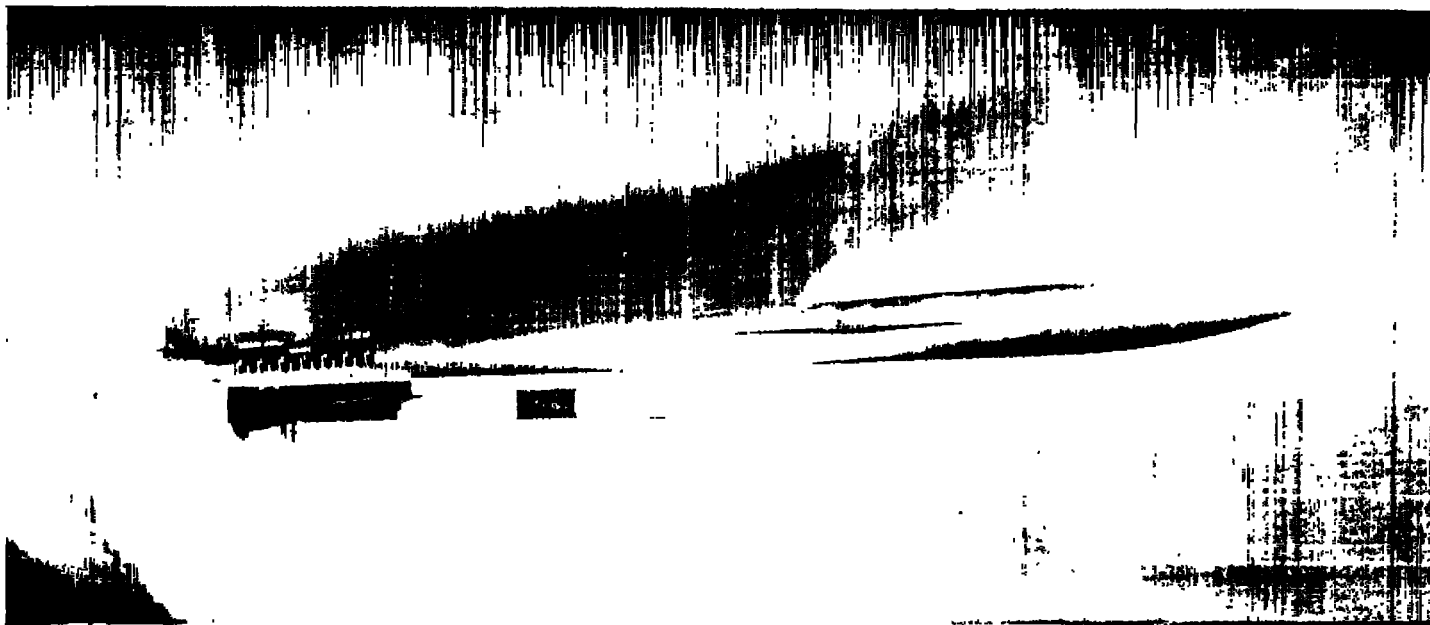
(a) Original model.

Figure 2.- Model details. All dimensions in inches unless otherwise noted.



(b) Vertical tail (shown at  $0.3b/2$  location).

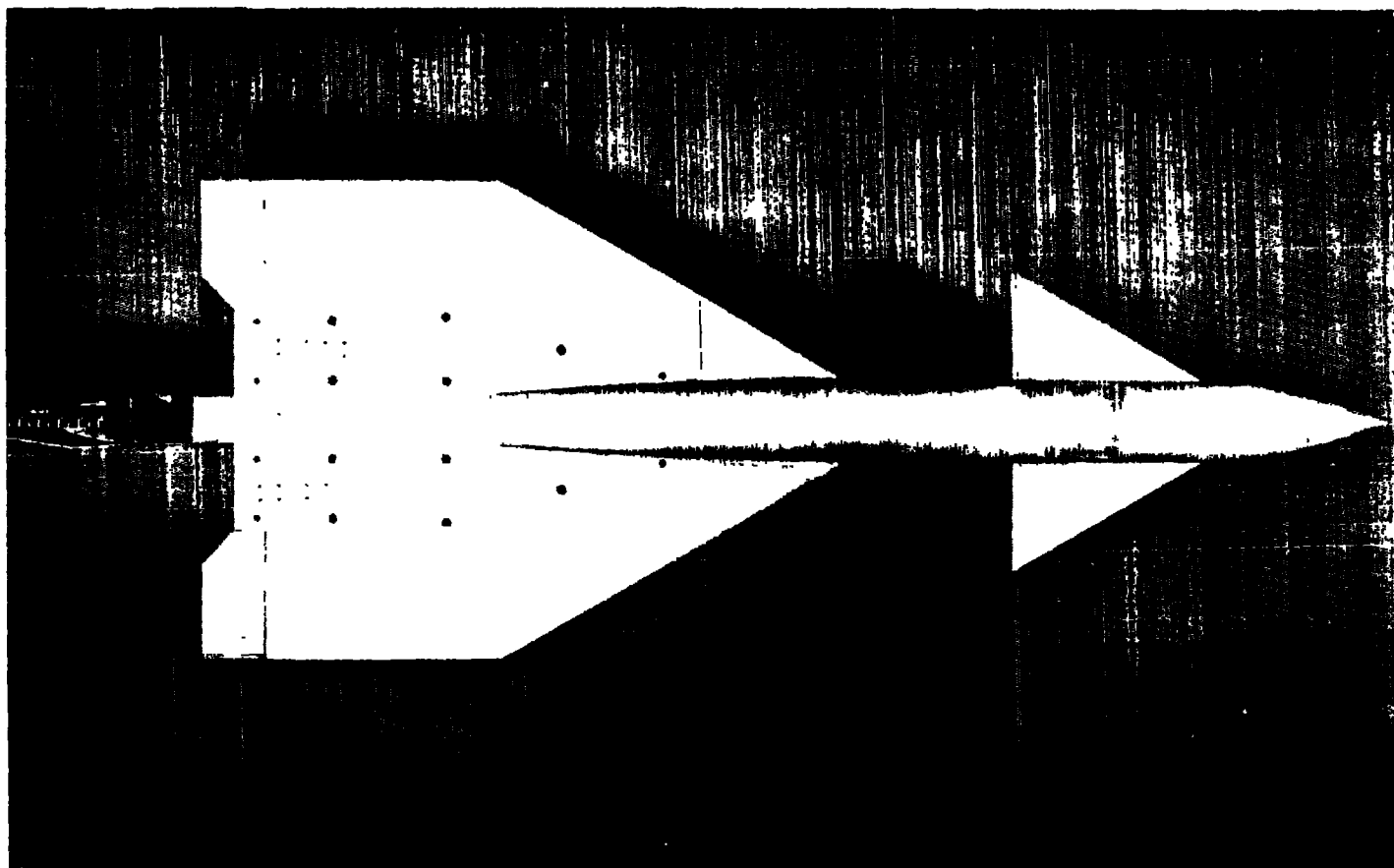
Figure 2.- Concluded.



(a) Three-quarter front view.

L-57-4321

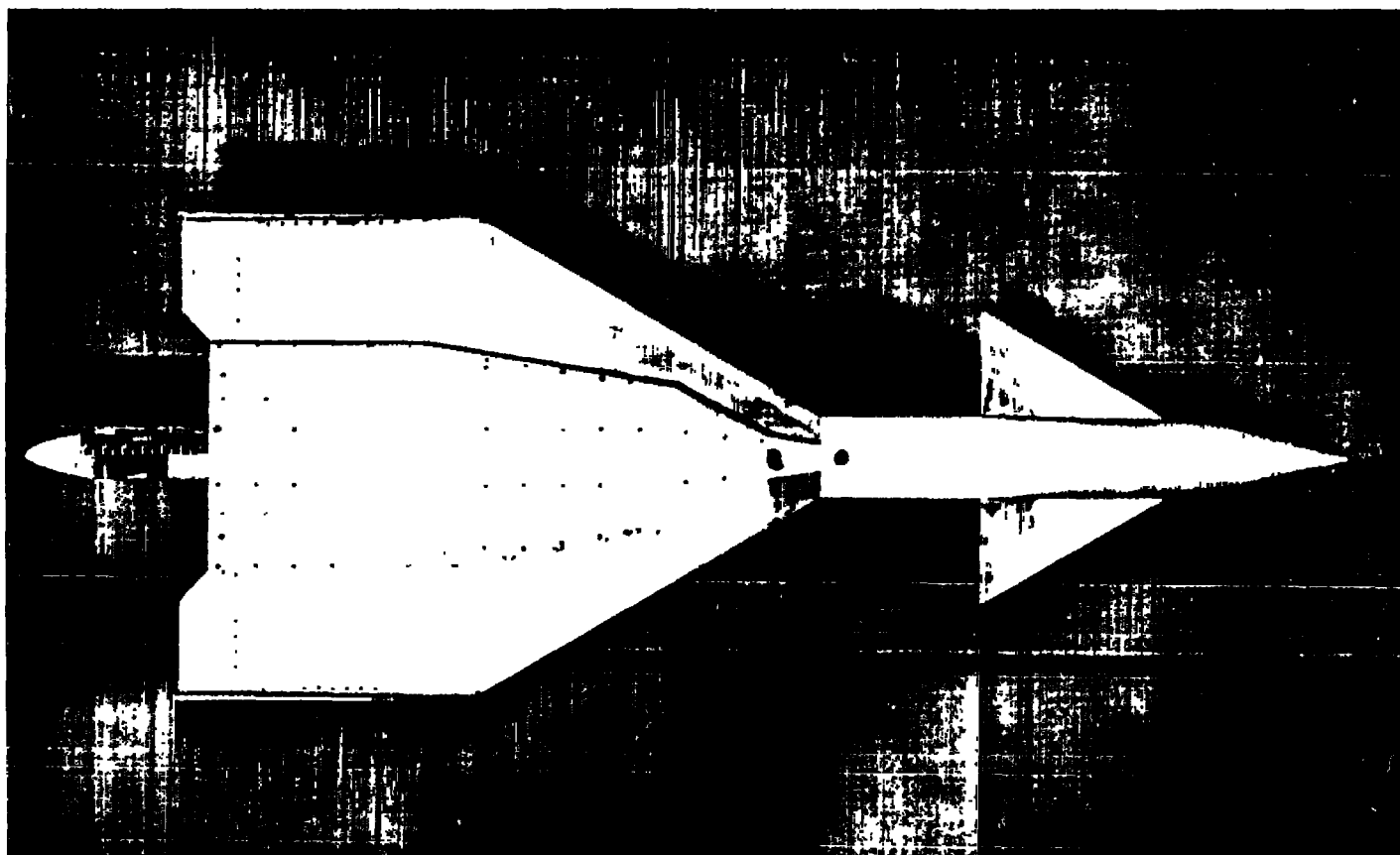
Figure 3.- Model photographs.



(b) Plan-form view, top.

L-57-4320

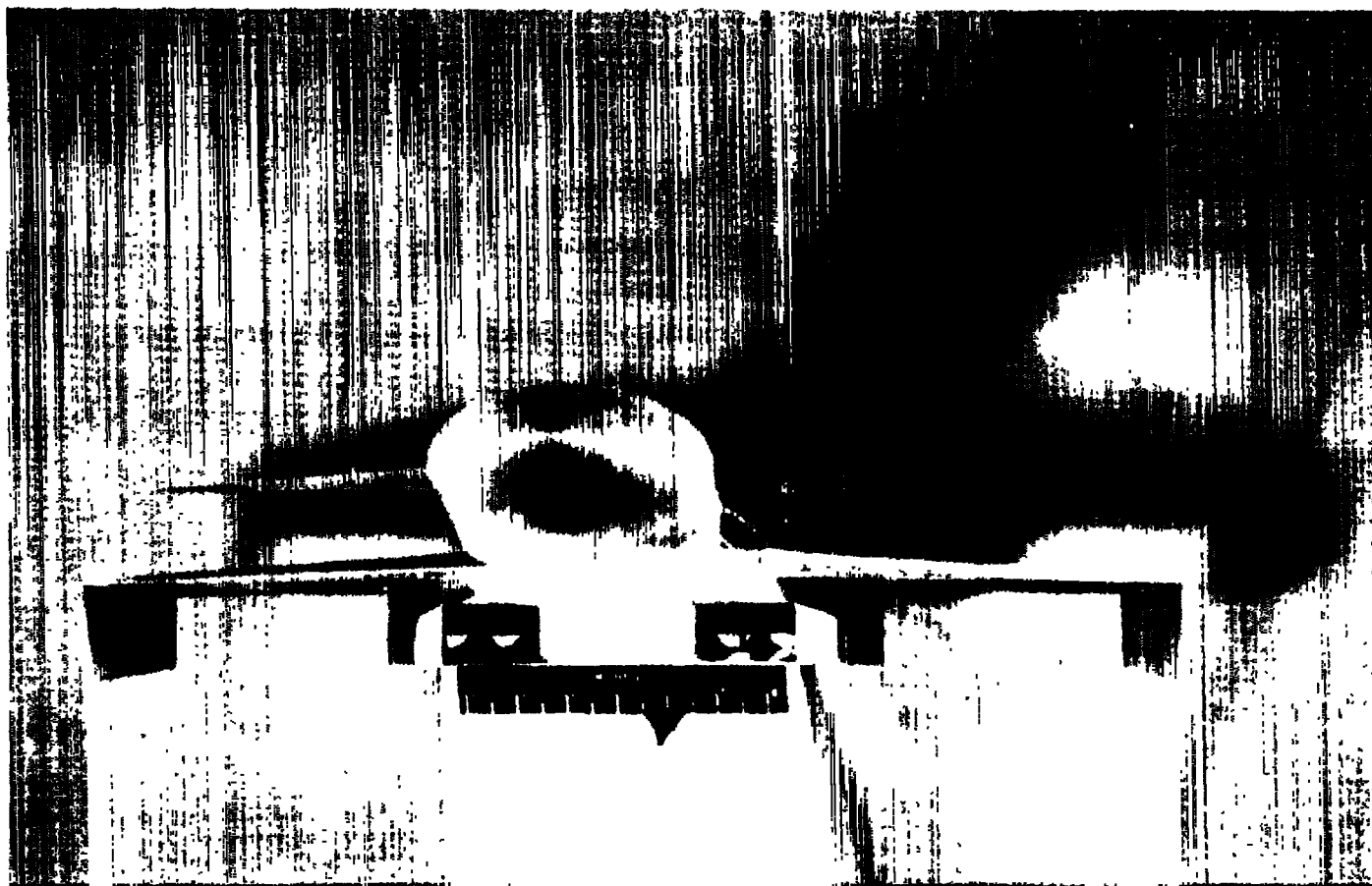
Figure 3.- Continued.



(c) Plan-form view, bottom.

L-57-4319

Figure 3.- Continued.



(d) Front view.

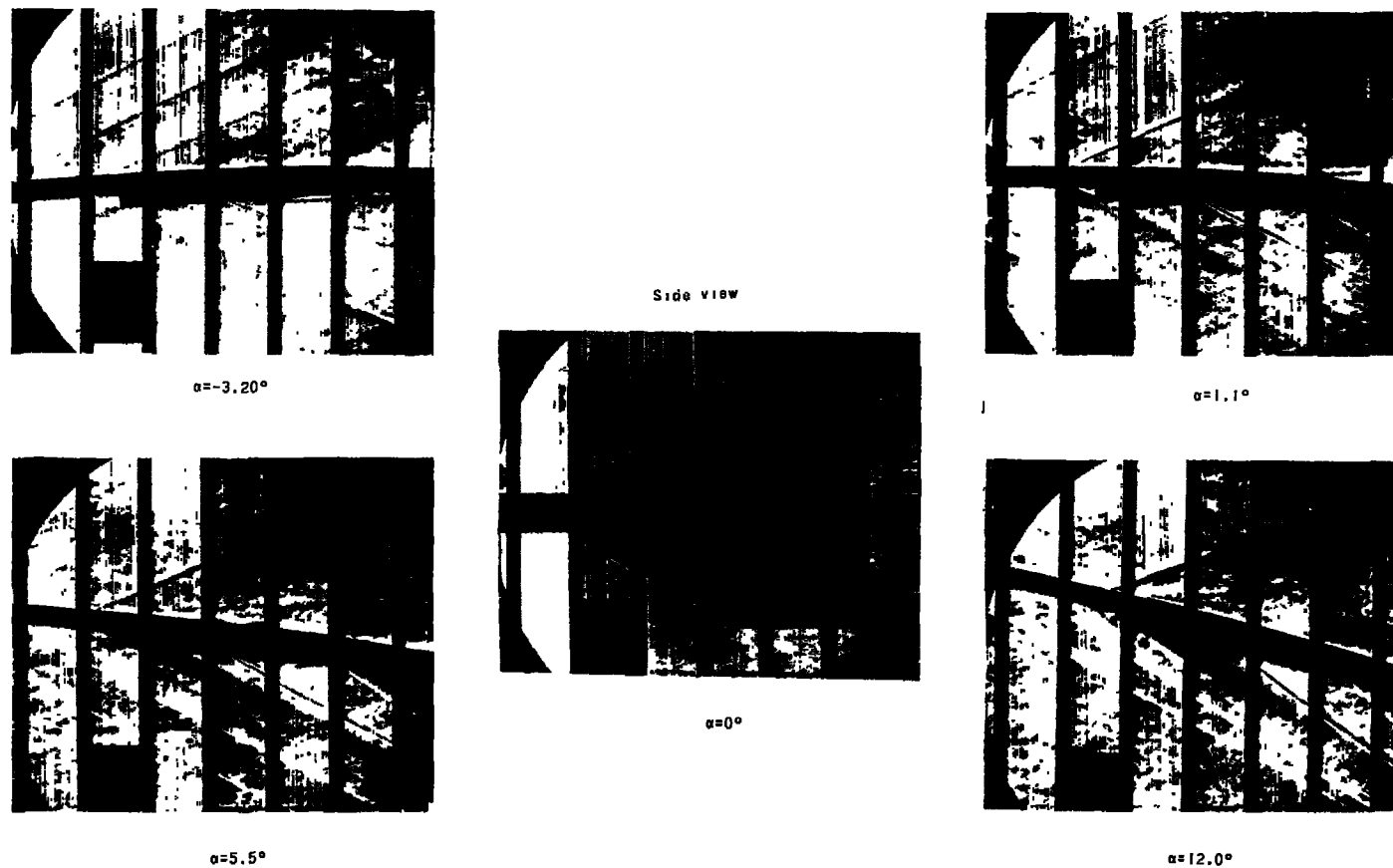
L-57-4323

Figure 3.- Continued.



(e) Ducting and boundary-layer diverter. L-57-4324

Figure 3.- Concluded.



(a)  $M = 2.50$ .

L-58-124

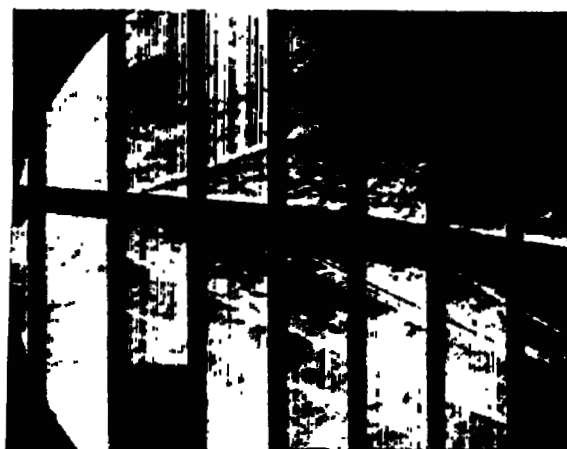
Figure 4.- Typical schlieren photographs of original model.  $\beta = 0^\circ$ .



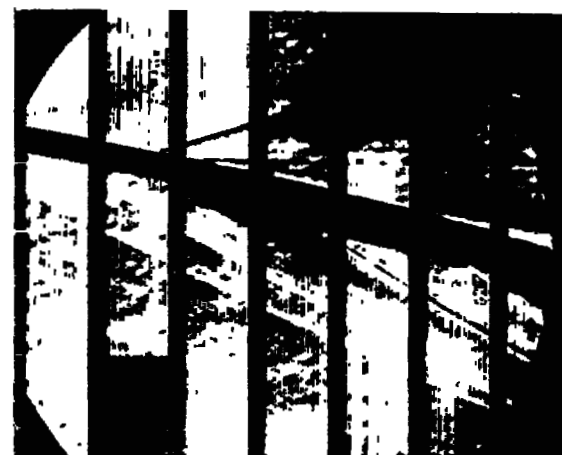
$\alpha = -4.1^\circ$



$\alpha = .2^\circ$



$\alpha = 4.4^\circ$



$\alpha = 10.6^\circ$

(b)  $M = 2.87$ .

L-58-125

Figure 4.- Concluded.

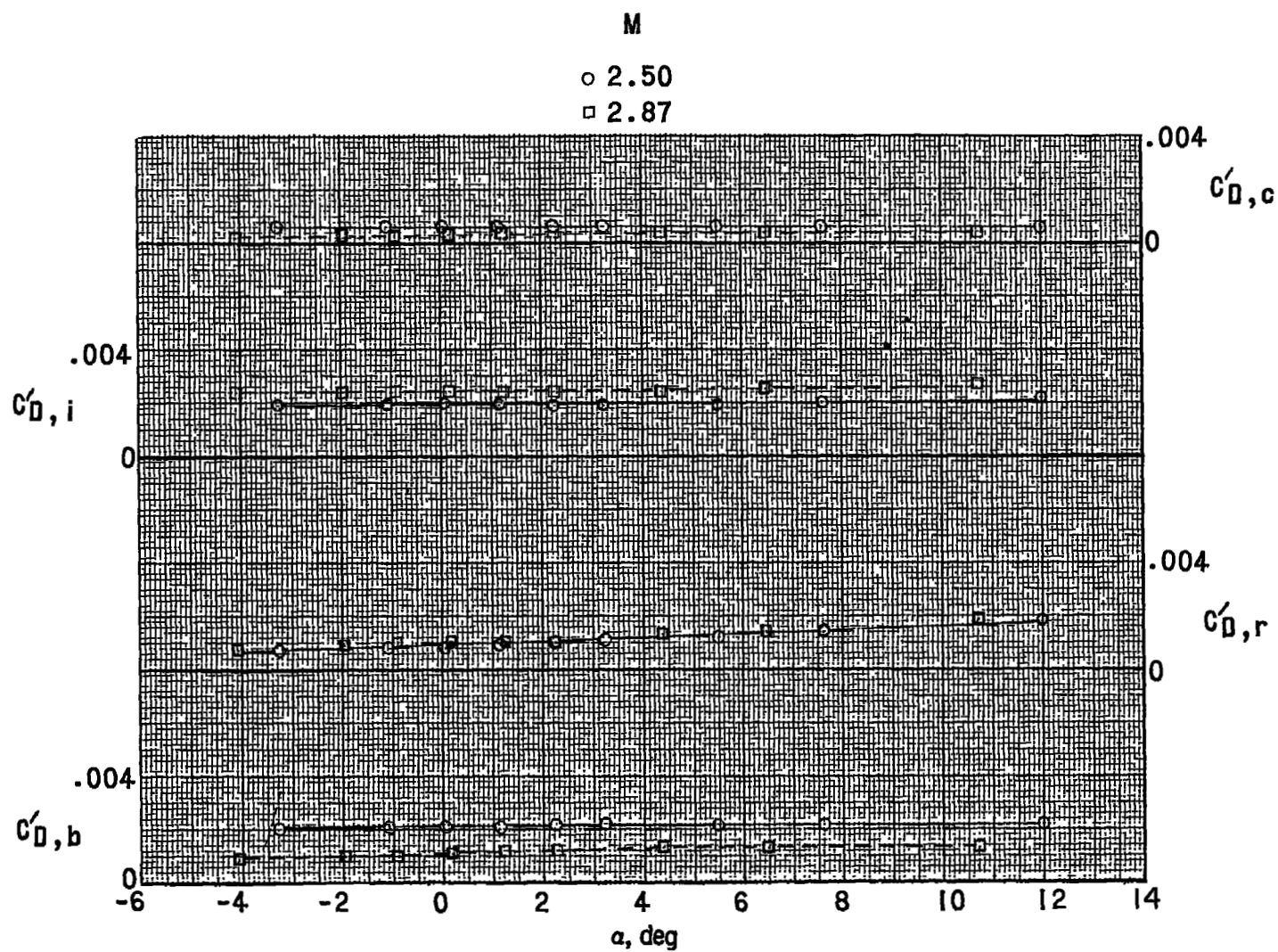


Figure 5.- Variation of internal, chamber, base, and ramp-pressure drag coefficient with angle of attack.

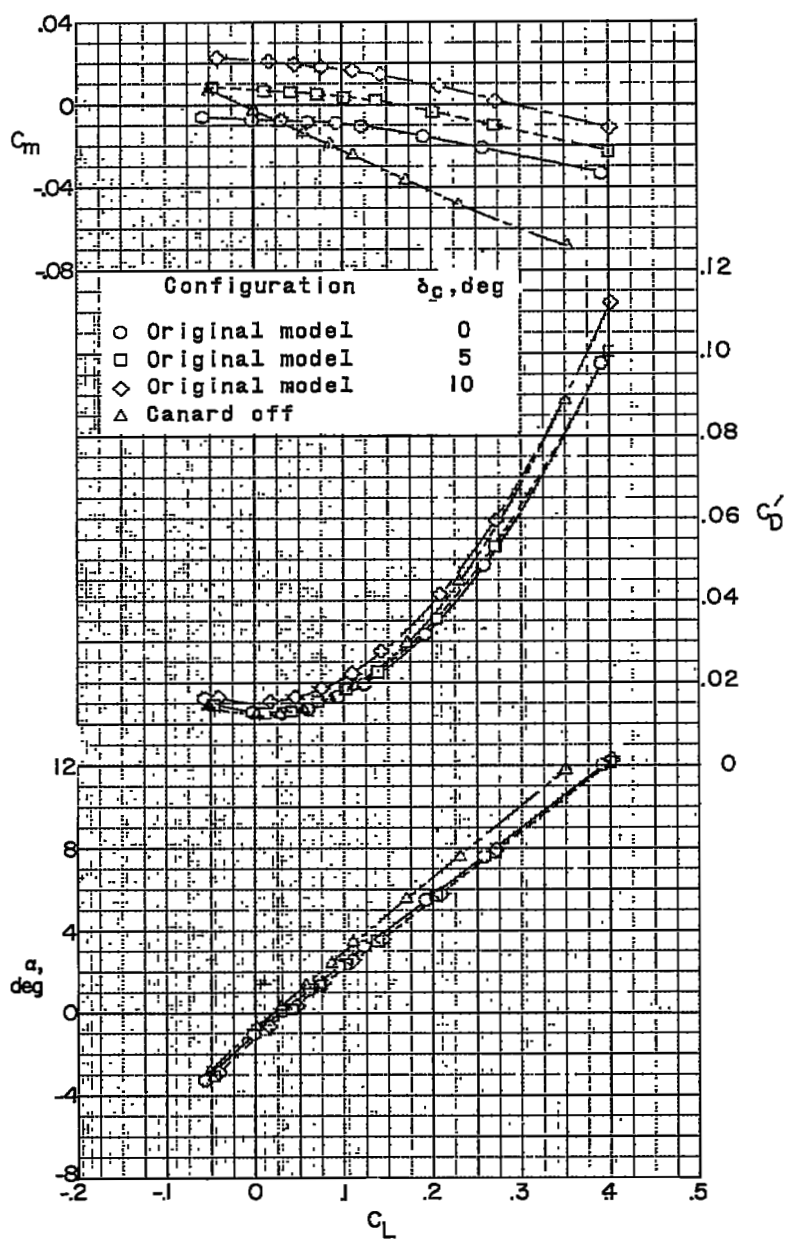
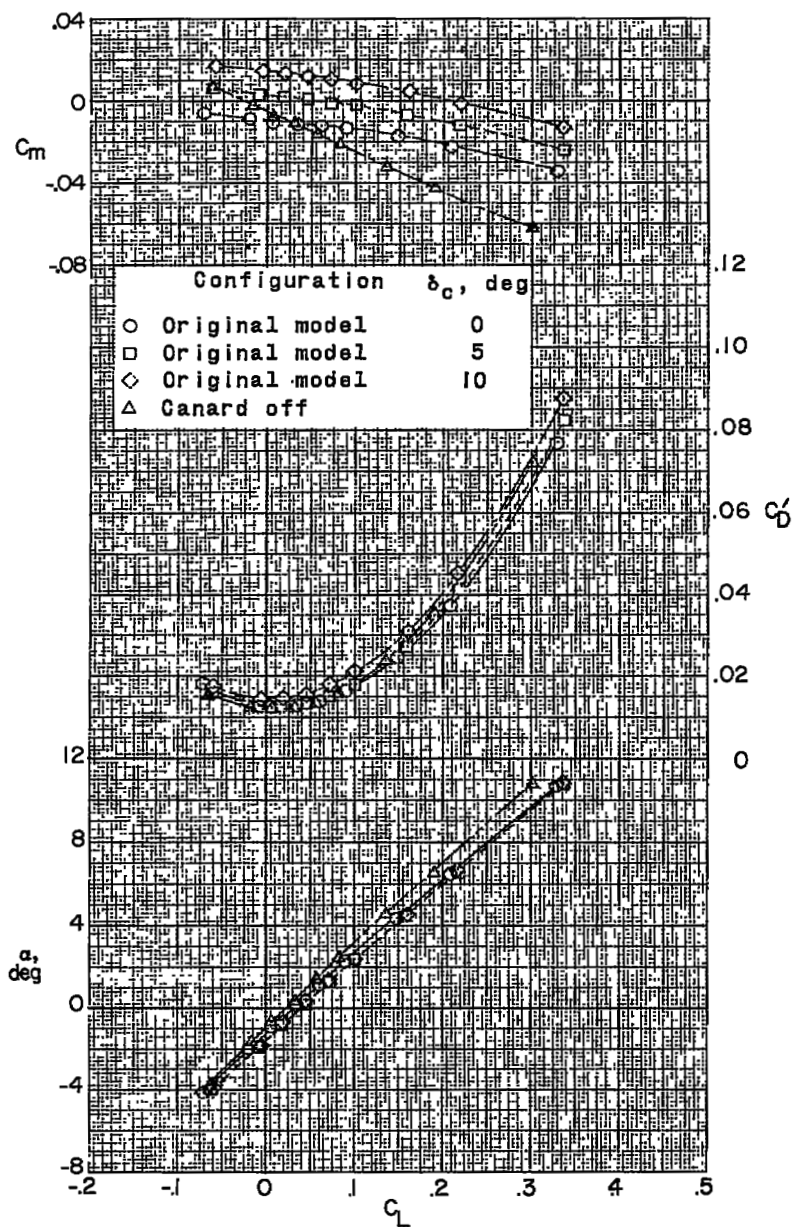
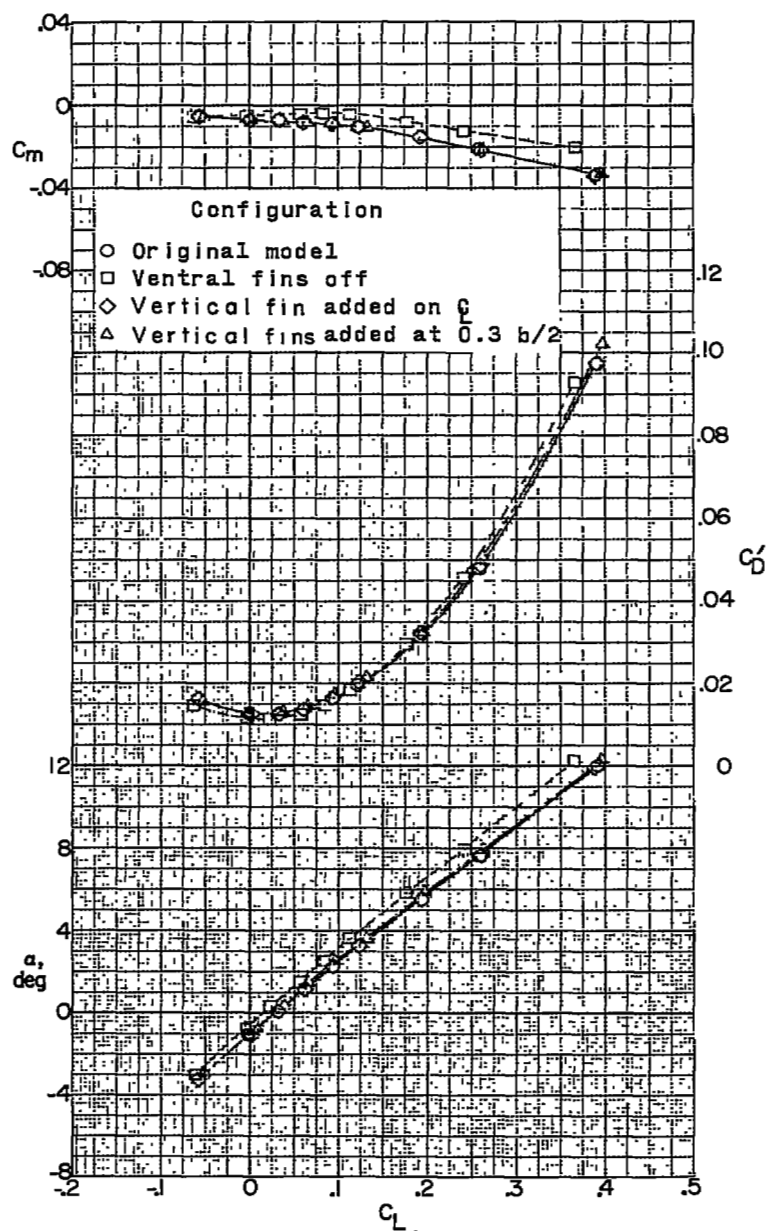
(a)  $M = 2.50$ .

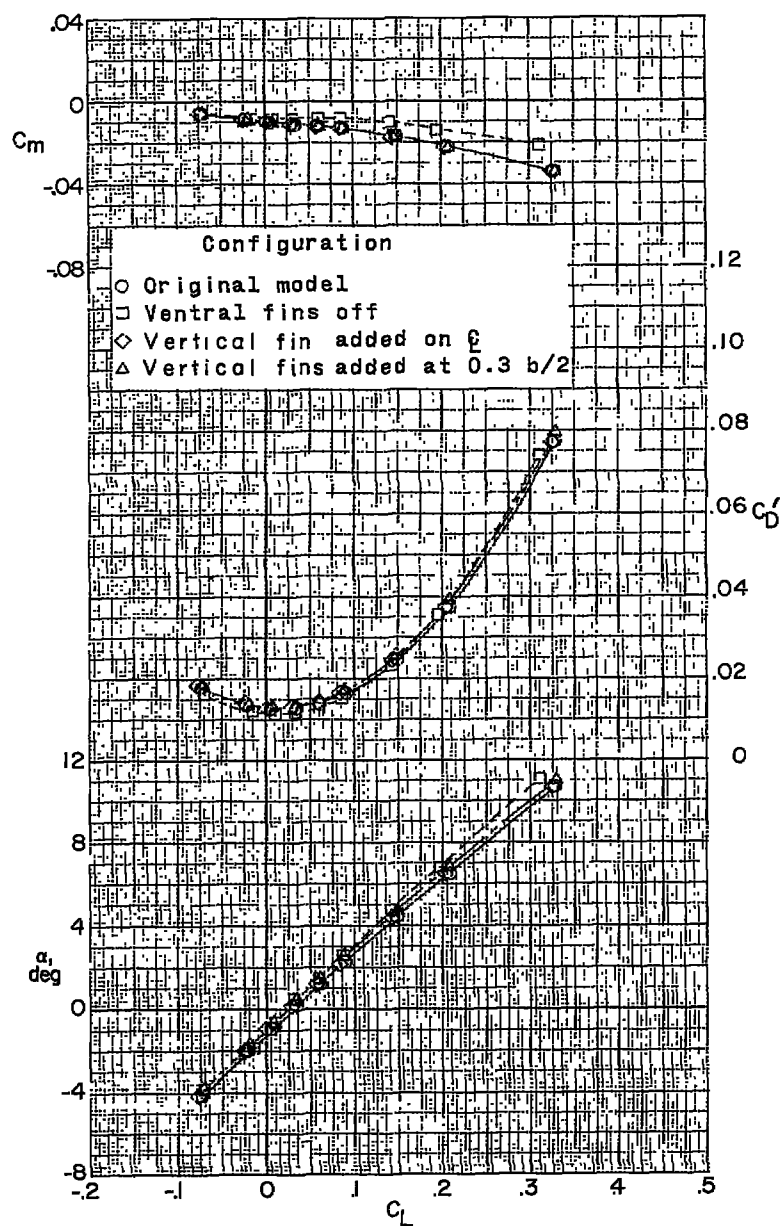
Figure 6.- Effect of canard on aerodynamic characteristics in pitch.



(b)  $M = 2.87$ .

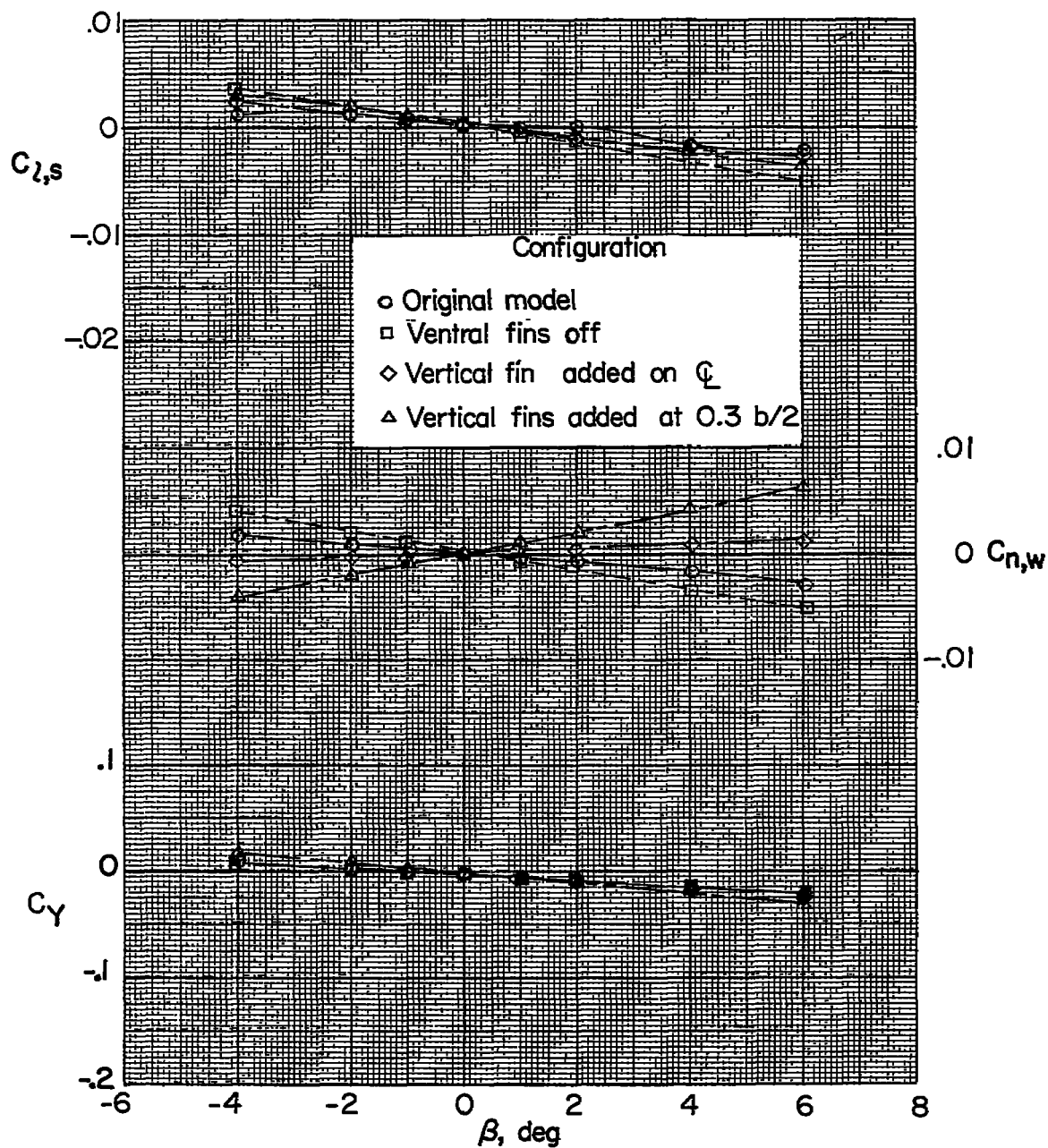
Figure 6.- Concluded.

(a)  $M = 2.50$ .Figure 7.- Effect of ventral and vertical fins on aerodynamic characteristics in pitch.  $\delta_c = 0^\circ$ .



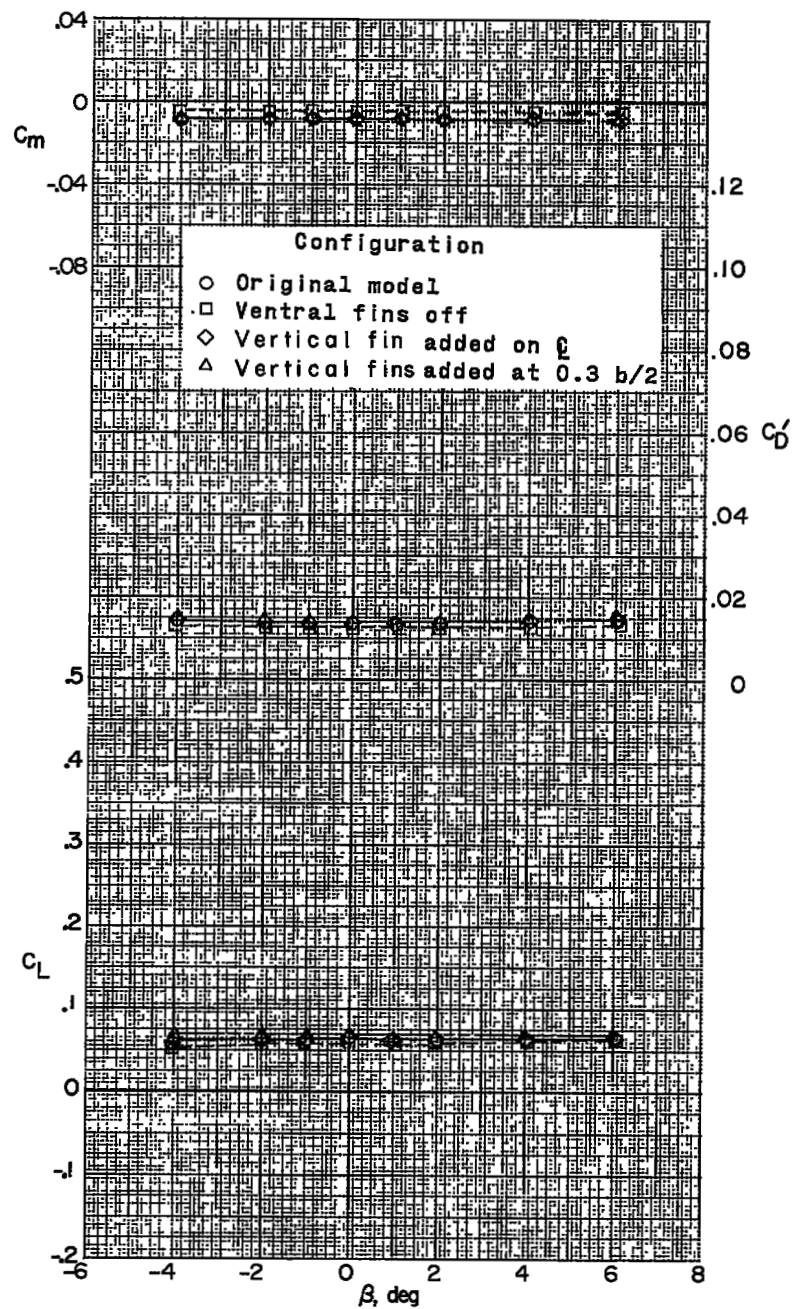
(b)  $M = 2.87$ .

Figure 7.- Concluded.



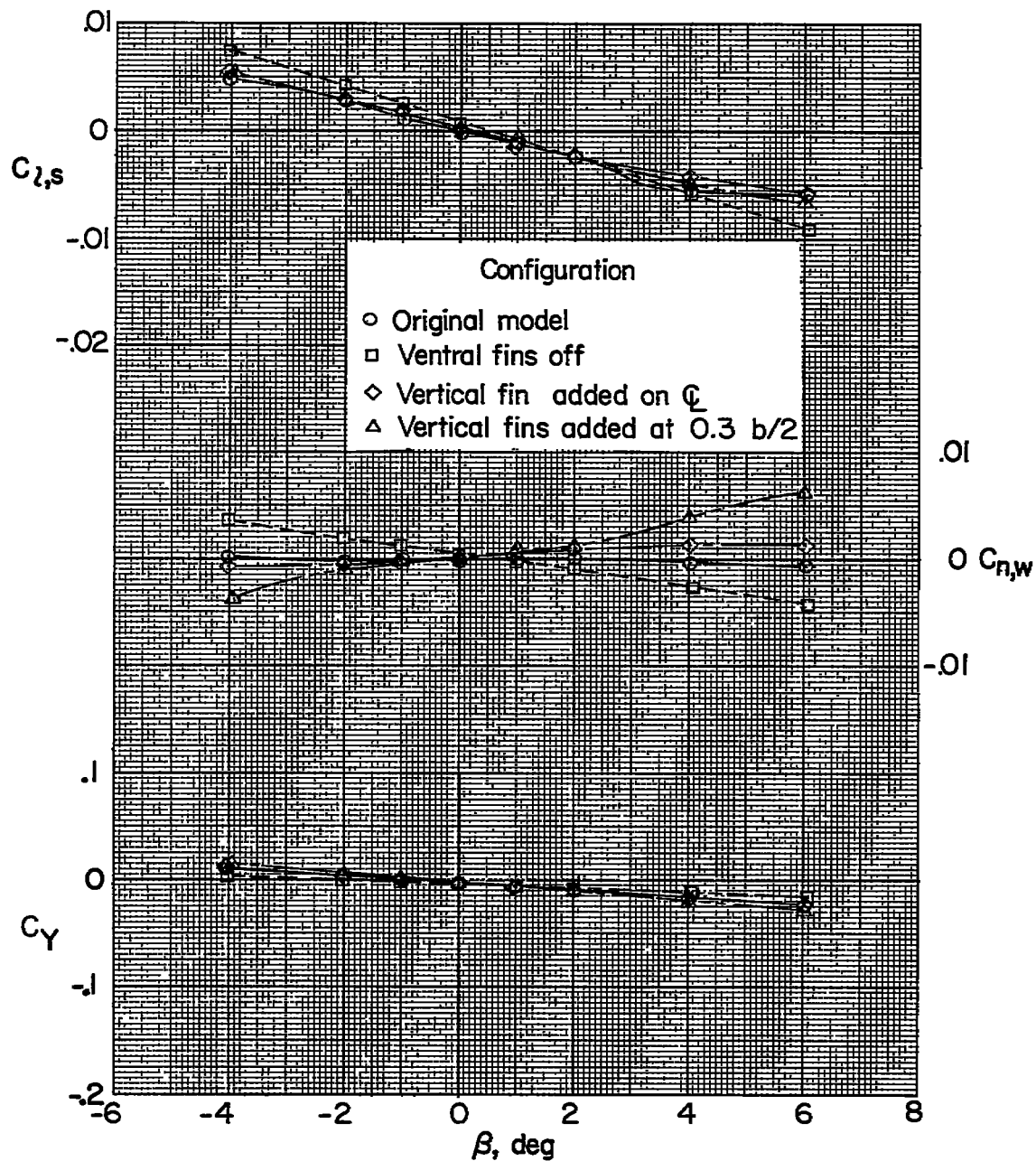
(a)  $\alpha \approx 1.1^\circ$ .

Figure 8.- Effect of ventral and vertical fins on aerodynamic characteristics in sideslip.  $M = 2.50$ ;  $\delta_c = 0^\circ$ .



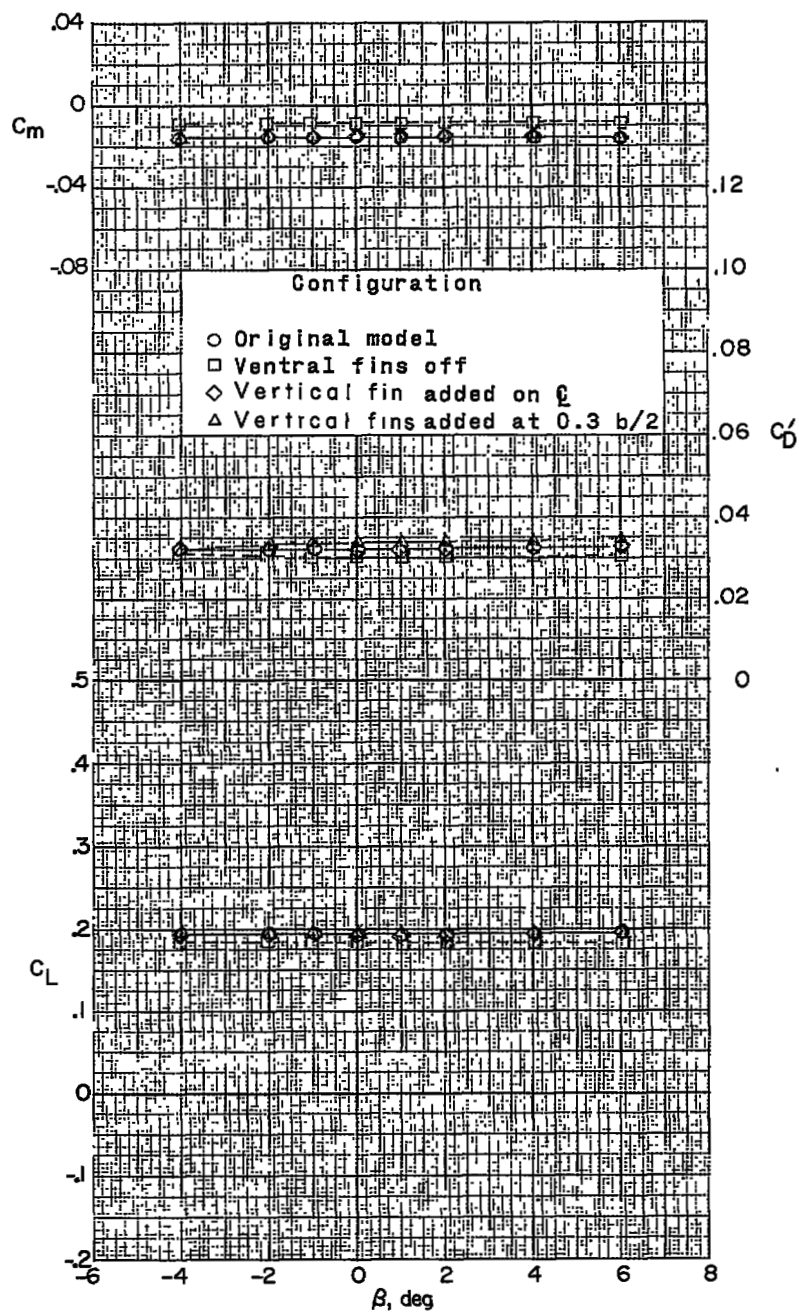
(a) Concluded.

Figure 8.- Continued.



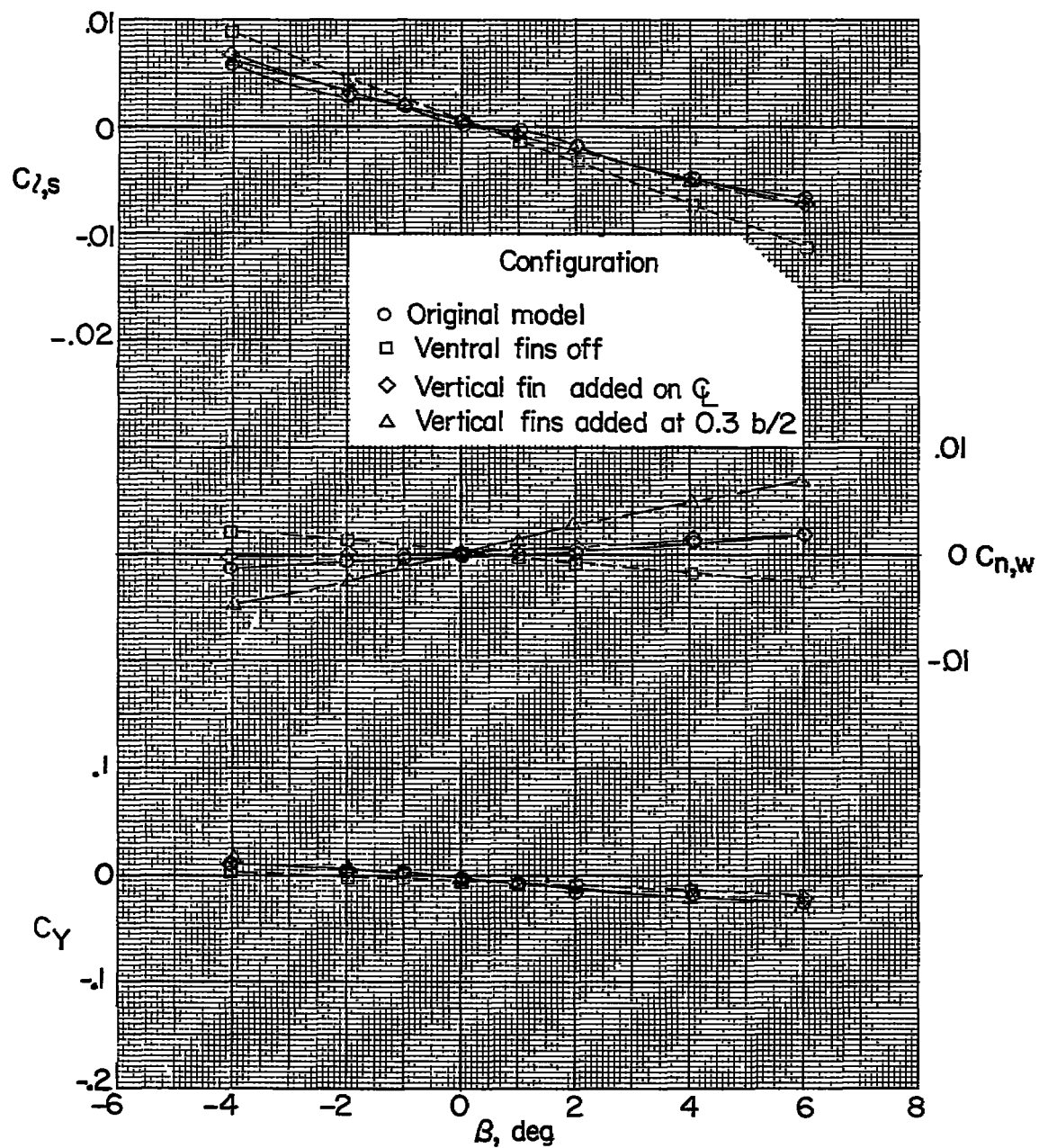
(b)  $\alpha \approx 5.5^\circ$ .

Figure 8.- Continued.



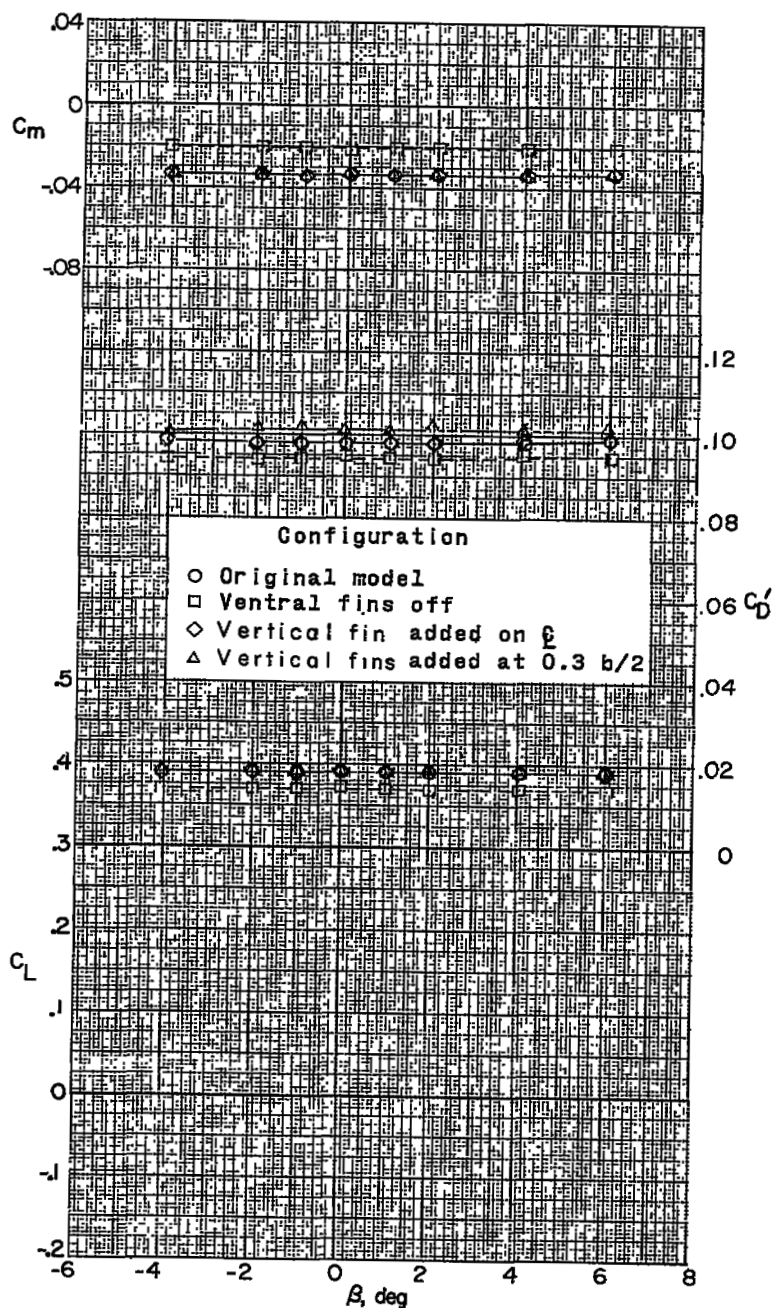
(b) Concluded.

Figure 8.- Continued.



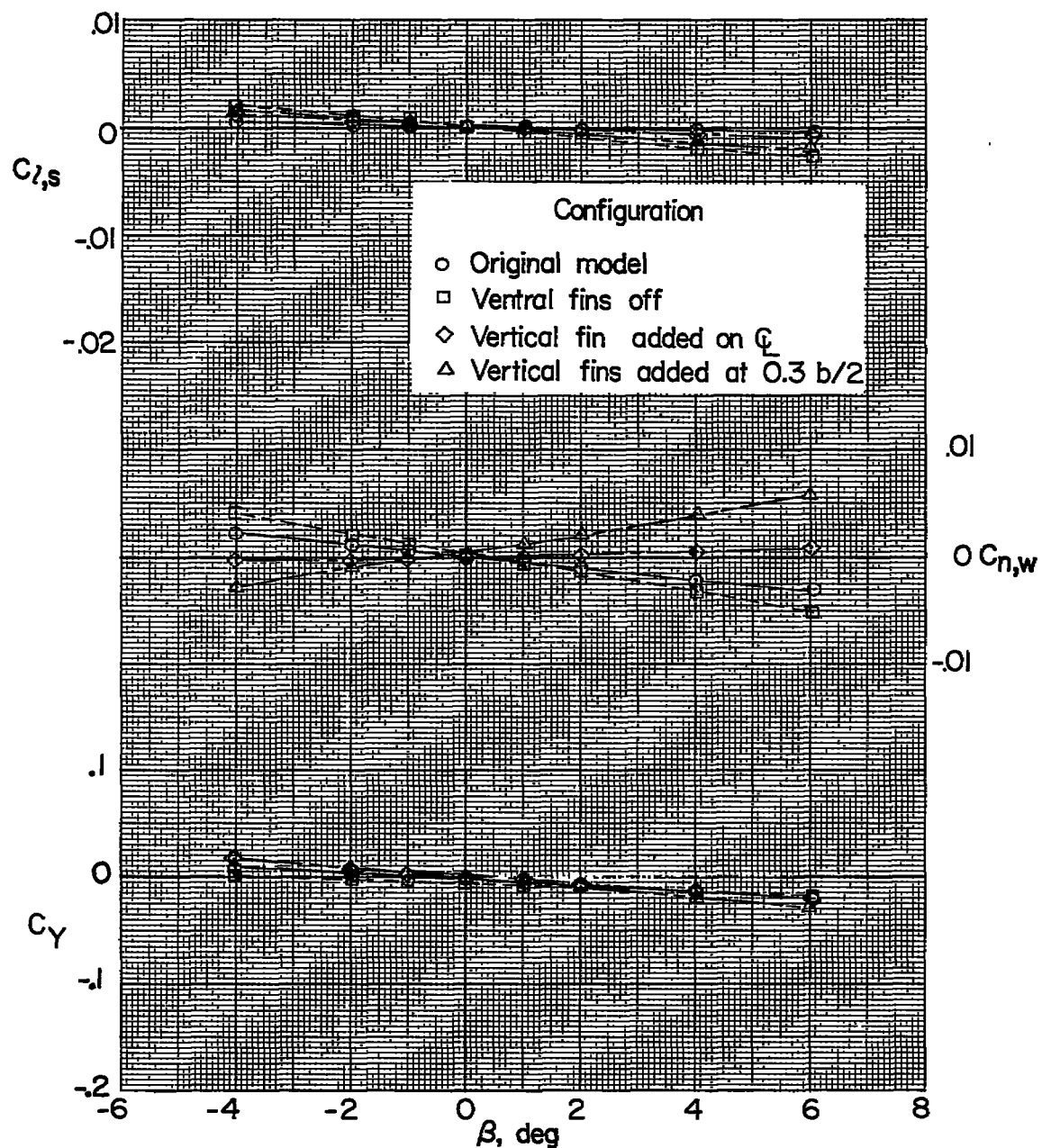
(c)  $\alpha \approx 12.0^\circ$ .

Figure 8.- Continued.



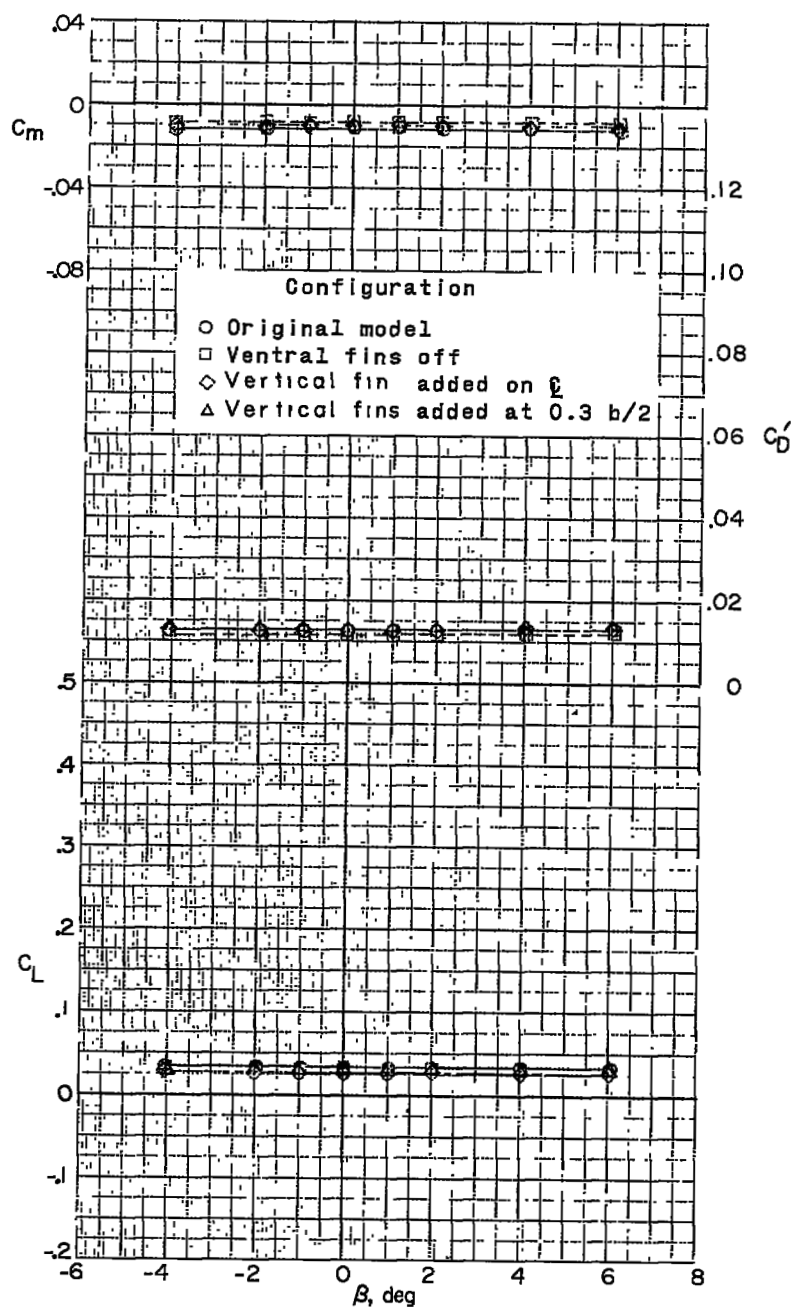
(c) Concluded.

Figure 8.- Concluded.



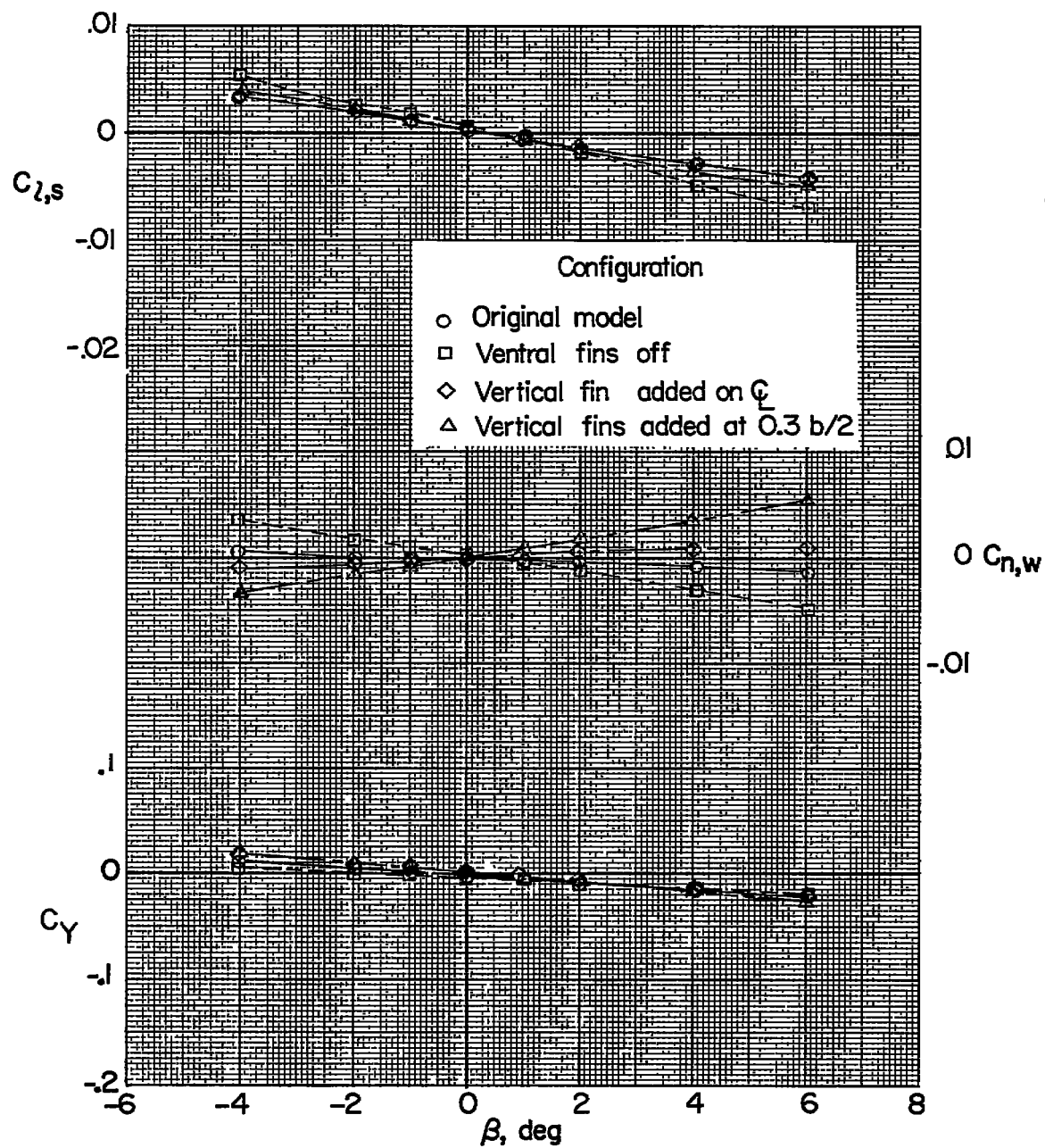
(a)  $\alpha \approx 0.2^\circ$ .

Figure 9.- Effect of ventral and vertical fins on aerodynamic characteristics in sideslip.  $M = 2.87$ ;  $\delta_c = 0^\circ$ .



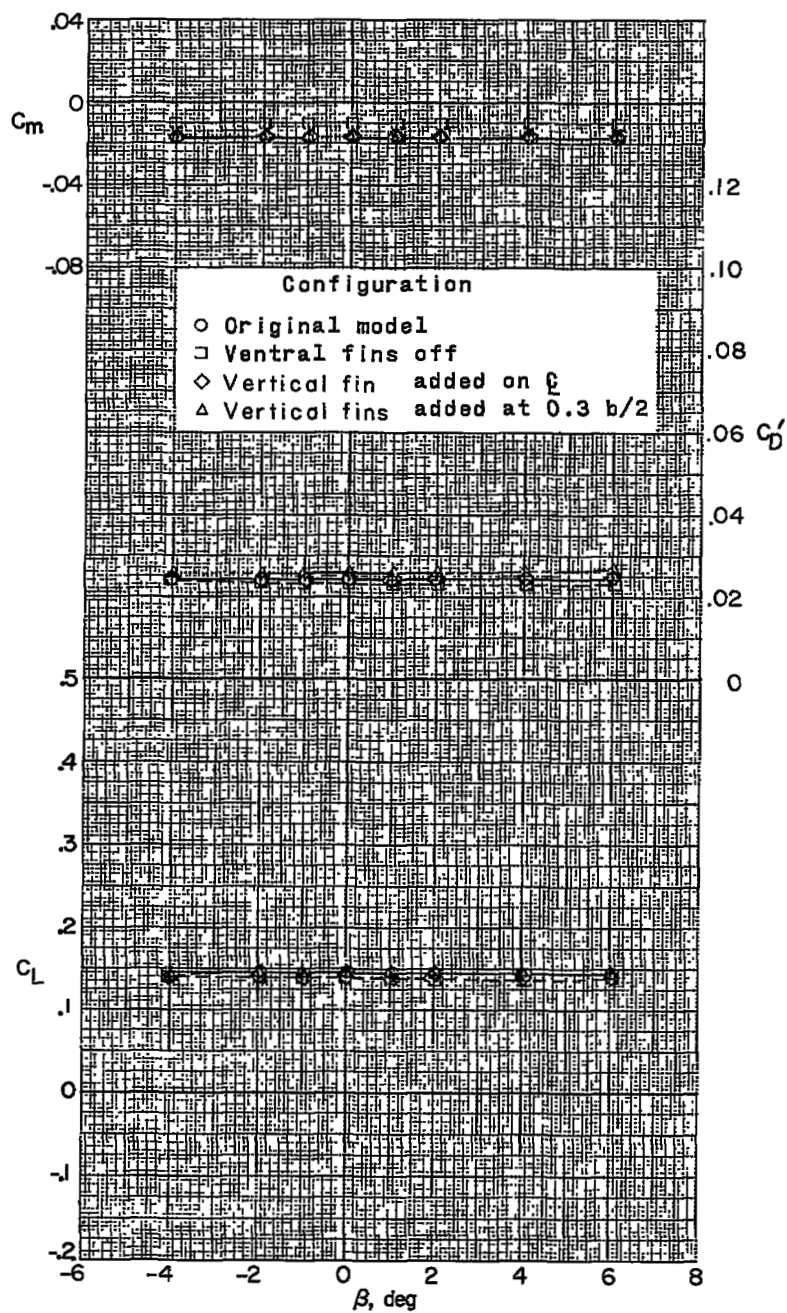
(a) Concluded.

Figure 9.- Continued.



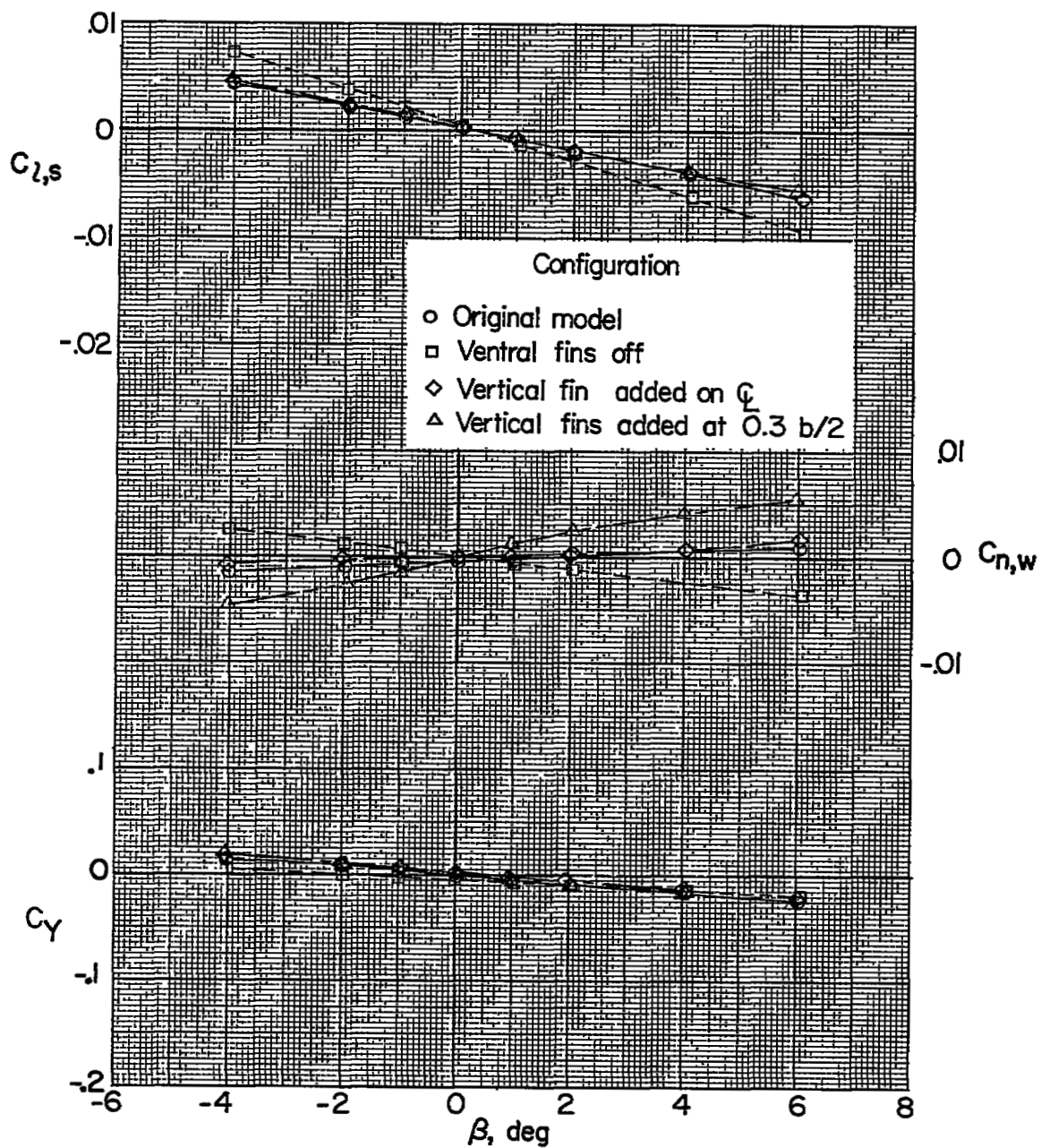
(b)  $\alpha \approx 4.4^\circ$ .

Figure 9.- Continued.



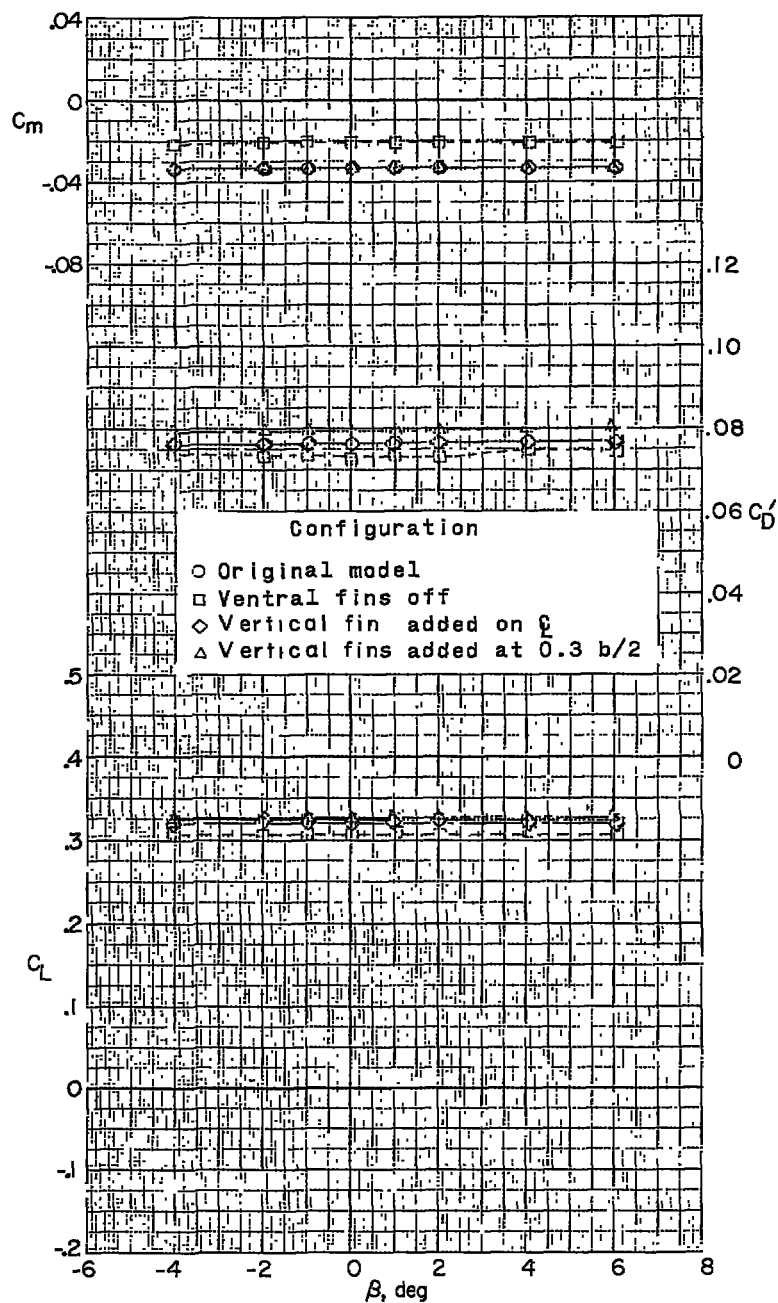
(b) Concluded.

Figure 9.- Continued.



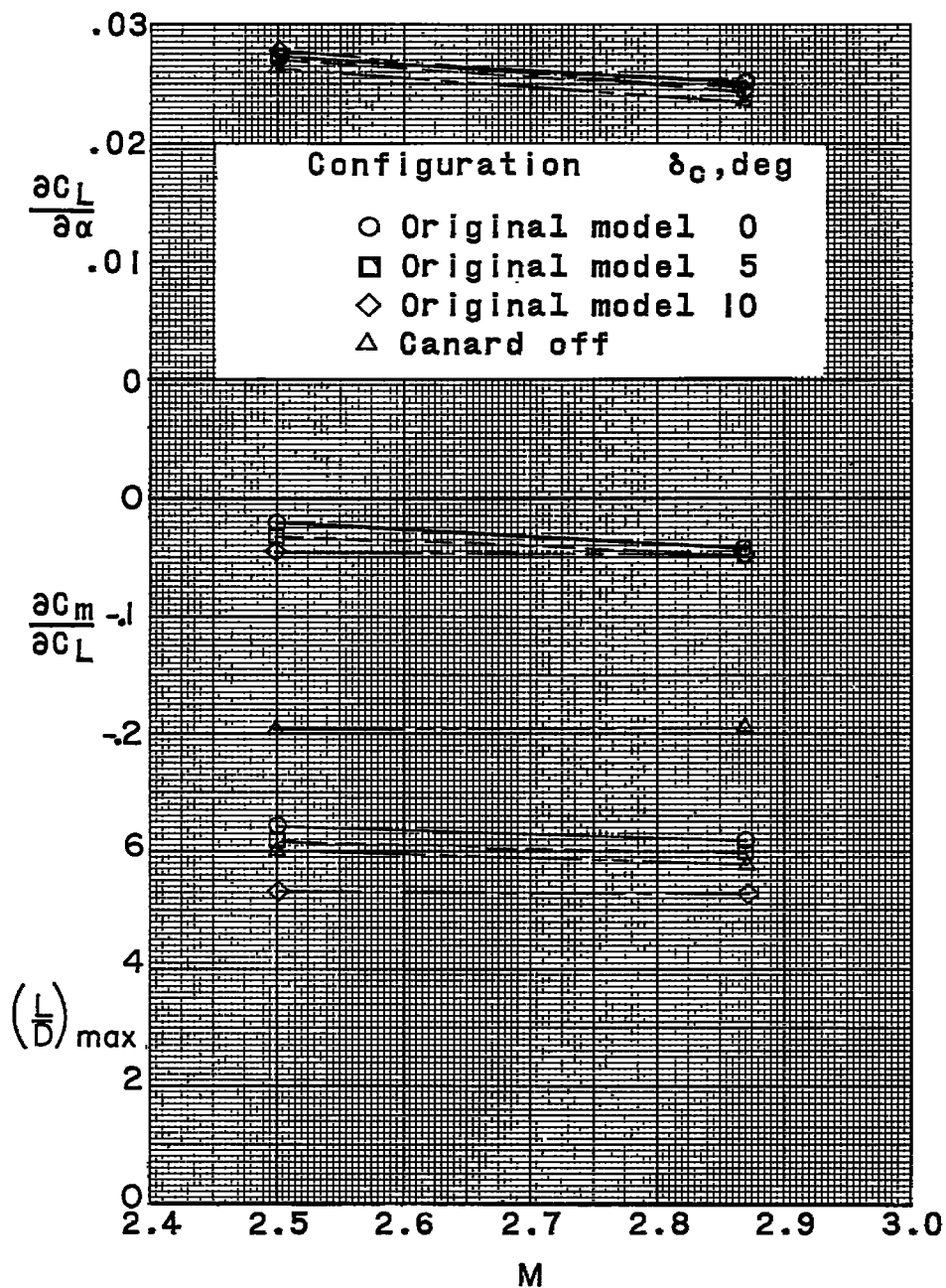
(c)  $\alpha \approx 10.7^\circ$ .

Figure 9.- Continued.



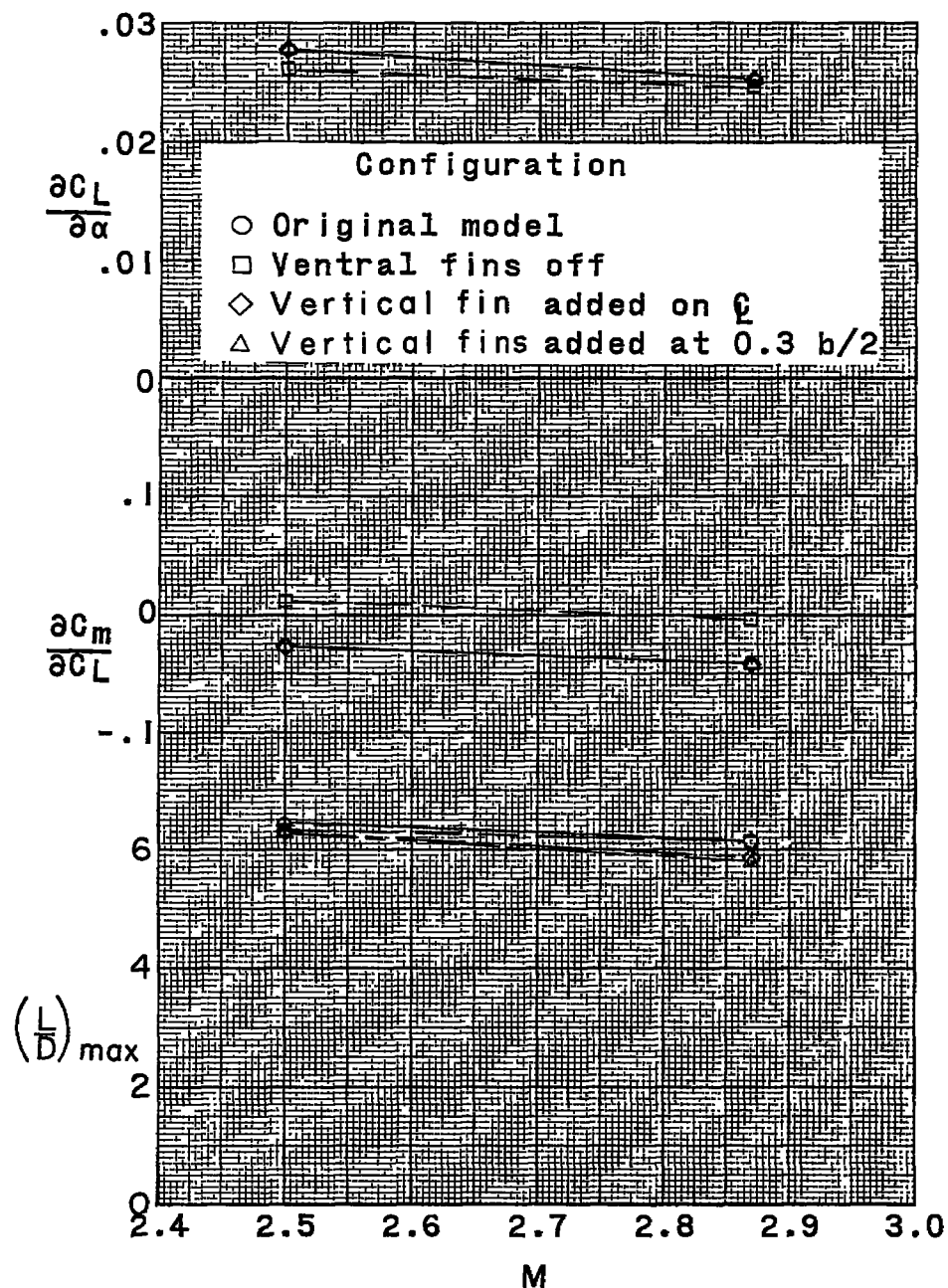
(c) Concluded.

Figure 9.- Concluded.



(a) Effect of canard surface.

Figure 10.- Summary of aerodynamic characteristics in pitch.



(b) Effect of ventral and vertical fins.

Figure 10.- Concluded.

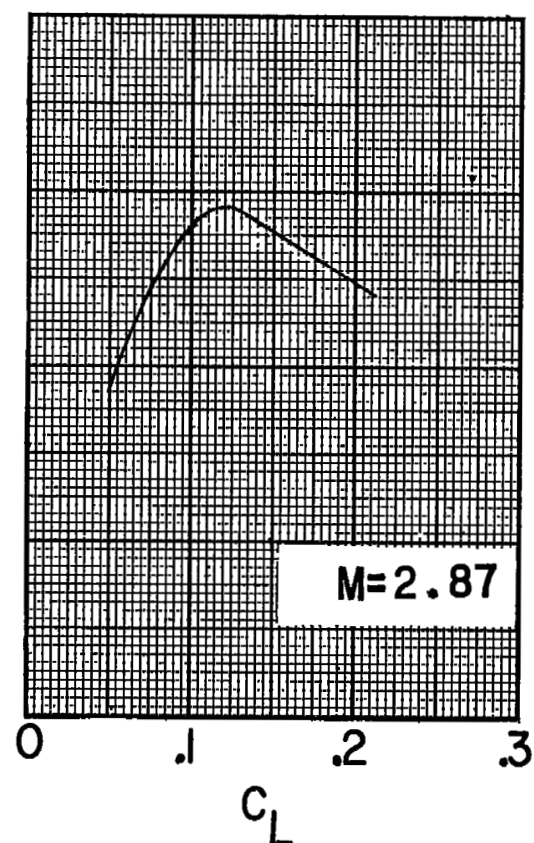
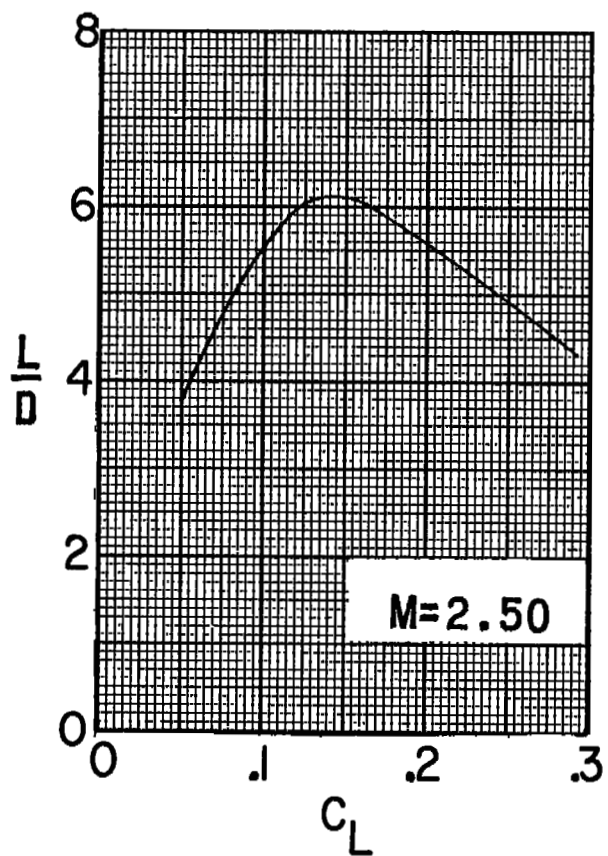


Figure 11.- Variation of trimmed  $L/D$  with lift coefficient.

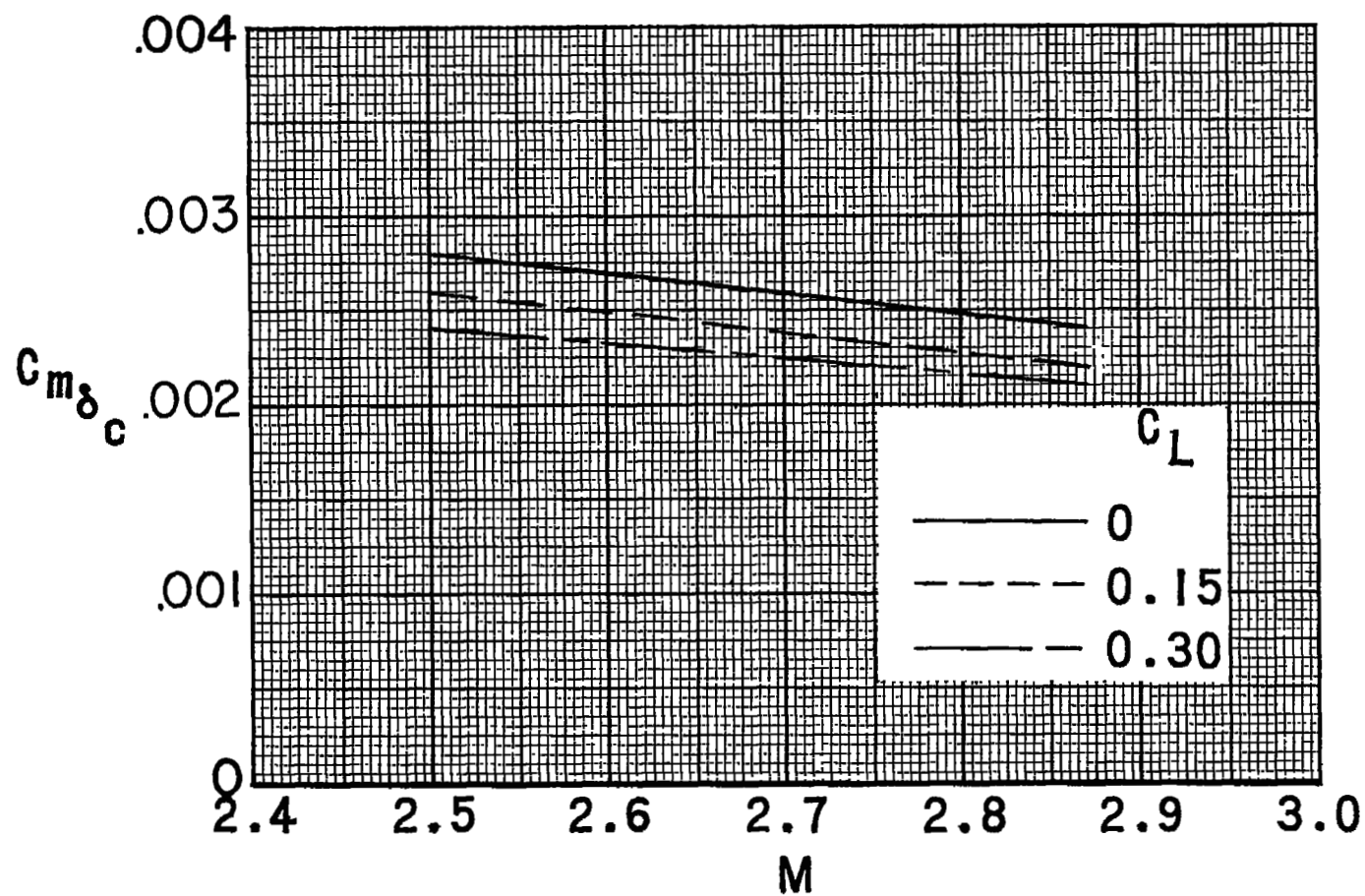


Figure 12.- Variation of canard effectiveness parameter with Mach number for several lift coefficients.

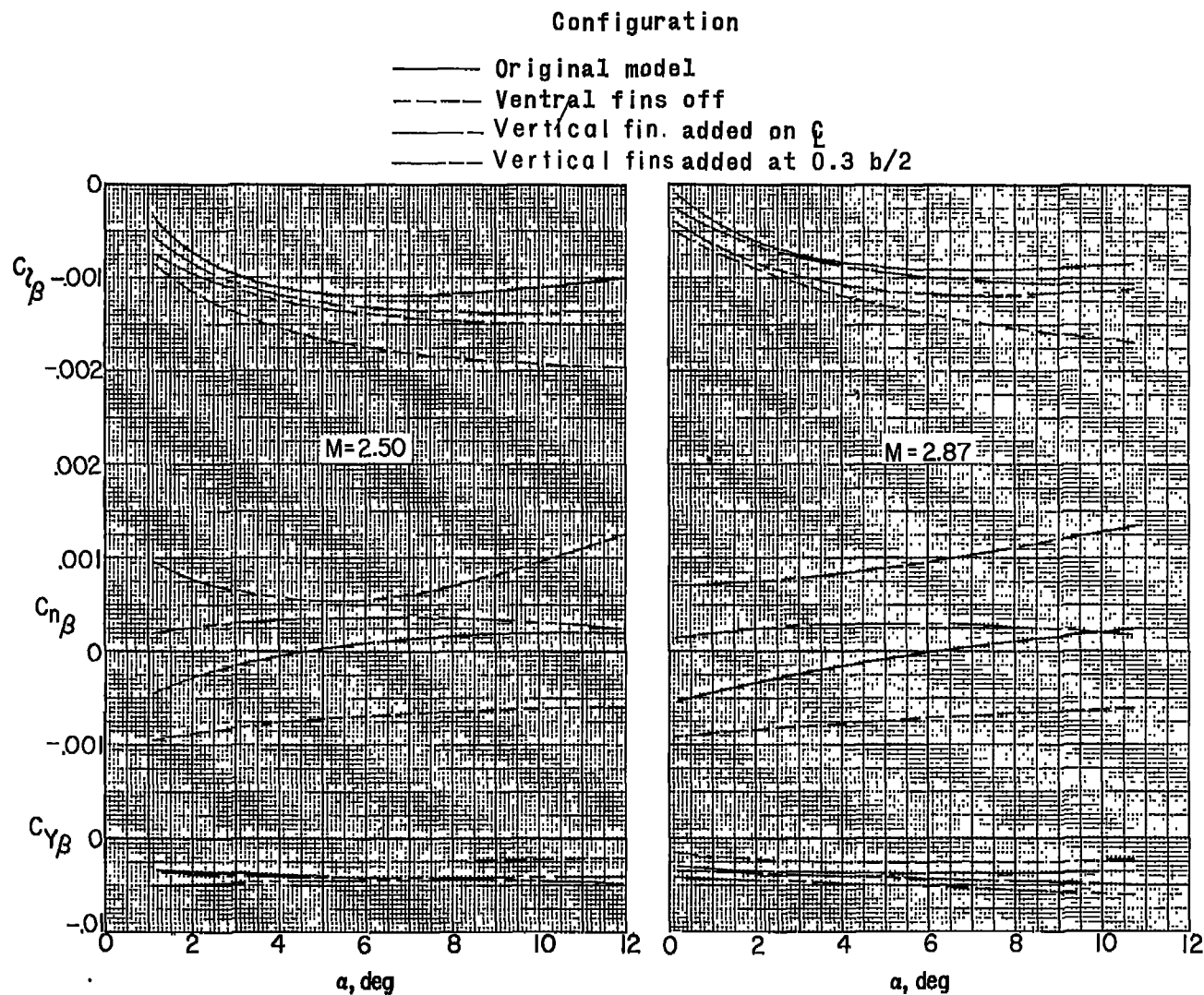


Figure 13.- Variation with angle of attack of the static lateral and directional stability derivatives.